EUROPEAN ORGANIZATION FOR NUCLEAR RESEARCH

A SEARCH FOR FRACTIONALLY CHARGED PARTICLES AT THE CERN INTERSECTING STORAGE RINGS

C.W. Fabjan, C.R. Gruhn*), L.S. Peak**),
F. Sauli and D.O. Caldwell***)

CERN, Geneva, Switzerland

L.S. Rochester†), U. Stierlin, R. Tirler,
B. Winstein††) and D. Zahniser†††)

Max-Planck-Institut für Physik und Astrophysik
Munich, Germany.

ABSTRACT

We report final results of a search for fractionally charged particles at the CERN Intersecting Storage Rings. Several independent scintillation counter, multi-wire proportional chamber (MWPC) telescopes simultaneously sampled centre-of-mass production angles from 0° to 90°. The experiment was sensitive to particles of electric charge in the range $0.1e < |Q| < 0.8e$, with velocities greater than 0.25c and with masses up to, in principle, 47 GeV/c^2. No such particles were observed among the products of 1.2×10^{10} proton-proton interactions at $s = 2830$ GeV^2. Our cross-section limit for the production of quark-antiquark pairs of charge $|Q| = 1/3e$ in the reaction $pp \to pp q\bar{q}$, at $s = 2830$ GeV^2, is $\sigma \lesssim 4 \times 10^{-35}$ cm^2 (90% confidence level) for quark masses up to ~ 20 GeV/c^2. For quarks with charge $|Q| = 2/3e$, the corresponding limit is $\sigma \lesssim 8 \times 10^{-35}$ cm^2, again for quark masses up to ~ 20 GeV/c^2.

Geneva - 31 July 1975
(Submitted to Nuclear Physics)

---

*) On leave from Michigan State Univ., East Lansing, Michigan, USA; supported in part by the Humboldt Stiftung, Sonderprogramm (USA), Germany.

**) Present address: Falkiner Nuclear Dept., Univ. of Sydney, NSW, Australia.

***) Present address: Physics Dept., Univ. of California, Santa Barbara, California, USA; supported in part by a Guggenheim Fellowship.

†) Present address: SLAC, Stanford, California, USA.

††) Present address: Enrico Fermi Inst., Univ. of Chicago, Illinois, USA.

†††) Present address: Laboratory for Nuclear Science, MIT, Cambridge, Mass., USA.

1. INTRODUCTION

It is an old, attractive idea to consider the strongly interacting particles as bound states of a few, "fundamental" objects[1]. The remarkable success of the SU(3) theory provided a new stimulus to consider this possibility, which found its expression in various models, such as fractionally charged "quarks"[2], or integrally charged triplets[3]. More recently, interest in these conjectures was renewed through the SLAC-MIT results on deep inelastic e-p scattering[4] and their interpretation with the "parton" model[5].

Based on these strong theoretical motivations, extensive experimental searches have been mounted to detect these particles, whether produced as secondary particles at high-energy accelerators, as a component of cosmic rays, or accumulated in terrestrial matter. So far, positive identification of such particles has eluded the experimentalist[6-11].

Figure 1 summarizes our knowledge of the limits on the quark production cross-section before the present experiment was undertaken (1972). Up to masses of ~ 5 GeV/c^2, the most sensitive limits were obtained in accelerator searches[9,10], whereas for heavier particles information came mostly from cosmic-ray work[6,8,11]. The interpretation of cosmic-ray flux limits in terms of cross-section limits is particularly model-dependent; we followed the work of Adair and Price[12] in the computation of the cosmic-ray limits of Fig. 1. The range of theoretical expectations for quark production cross-sections is also indicated in Fig. 1. For the diffraction-like process $pp \to p + 3q$, cross-sections in the submillibarn range are predicted[13], which for asymptotic energies become mass independent. For the opposite extreme we show an estimate based on the thermodynamical model[14,15]. The scaling prediction for the production and dissociation into $q\bar{q}$ pairs of heavy, virtual photons[16] might eventually be accessible to experimental tests.

The CERN Intersecting Storage Rings (ISR) have extended up to ~ 60 GeV the centre-of-mass energy available for the controlled production of new particles. This is considerably beyond the 12 GeV Serpukhov limit[10] or the 25 GeV NAL limit[17] and corresponds at its highest energy to an 1800 GeV/c beam hitting a stationary target. While the mass range can be extended appreciably at the ISR, the cross-section limits cannot be pushed so low as at conventional accelerators. The rate R of interactions, and therefore the cross-section limit is characterized by the luminosity $L = R_{total}/\sigma_{total}$, which during 1972 was close to the design luminosity of $L_{design} = 4 \times 10^{30}$ interactions/cm^2 sec. At an accelerator, the same rate would be obtained from only 10^6 protons/sec impinging on a 60 cm long liquid-hydrogen target or from $\sim 10^5$ protons/sec on a 30 cm long beryllium target. As a result of this comparatively low luminosity, cross-section limits measured at the ISR will be at a level of about 10^{-35} cm^2, compared to limits of less than 10^{-40} cm^2, achievable at accelerators.

We report here our final results[18] of a search for particles with electric charge Q in the range $0.1e < |Q| < 0.8e$; since the properties of our detector depended to some extent on the charge of the particles, we will frequently discuss the special cases $|Q| = 1/3e$, and $2/3e$. The next section outlines the design of the apparatus and the precautions taken to reach a sensitivity of $\sigma \sim 10^{-35}$ cm^2, which requires a detector capable of identifying one quark amongst 10^{10} normal ($|Q| = 1e$) particles. In subsequent sections we describe in detail the detector, its associated electronics, detection capabilities, and acceptance characteristics. After the discussion of the data analysis our results will be given in terms of flux limits and cross-sections are derived within the framework of two plausible models.

2. DESCRIPTION OF THE DETECTION SYSTEM

2.1 Detection principle

As in previous counter experiments[9,10], the detection of fractionally charged particles is accomplished through simultaneous measurements of the specific energy loss (dE/dx) and the particle velocity β. For particles with masses $M >> m_e$, the electron mass, we can express to a very good approximation the most probable value of the energy loss ε_p in the form

$$\varepsilon_p = Q^2 \cdot f(Q^2,\beta).$$

Because the energy loss is velocity-dependent and subject to statistical fluctuations, several independent measurements of dE/dx and a measurement of β are necessary to provide a statistically significant determination of the absolute value of the charge $|Q|$. Furthermore, the expected consistency of multiple measurements of dE/dx provides a powerful tool for rejecting certain types of background events which might simulate fractionally charged particles.

Initial studies with a telescope consisting of nine $10 \times 10 \times 1$ cm^3 scintillators were carried out in a 10 GeV/c test beam at the CERN Proton Synchrotron (PS) and at the ISR. In the relatively clean background conditions of the PS beam, we found that a rejection power better than 10^9 could be achieved with such a system (no quark-like event among 10^9 charged particles passing through the telescope). The final design of the telescopes minimized the following classes of background events:

i) Edge effects: normal particles can simulate quarks if they traverse the counters close to an edge (within 5 mm), resulting in a low level of scintillation light collected at the photomultipliers (PM's). Consequently, the geometry of the counters was chosen in such a way that in any direction no more than three edges of different counters were aligned within 5 mm.

ii) Čerenkov effect in light-guides: the passage of a fast particle through conventional lucite light-guides can simulate low dE/dx events through Čerenkov-light production. We therefore adopted a design in which the end of the scintillator was tapered to match the PM's (Fig. 2). Normal particles passing through this scintillator light-guide produce a very high light output and no longer constitute a source of low pulse-height-background. The counters were viewed by 56 DVP PM's, which yielded between 200 and 500 photoelectrons for a minimum ionizing particle (min.I. : $|Q| = 1e$, $\beta = 0.96$), depending on counter size.

iii) Čerenkov effect in PM glass envelope: low pulse height events can be produced by fast particles traversing the PM's. Protection with small anticounters was found to be sufficient.

2.2 Layout of the detector in intersection I4

Six telescopes were installed at the ISR in intersection I4, as shown in the scale drawing Fig. 3. All counters were designed as indicated above, with the exception of the five largest counters of telescope L (up to 32×100 cm^2) which were viewed by two PM's each. The telescopes were mounted in the plane of Beam 1 and Beam 2, except for telescope A, which was placed on top of the vacuum pipe in order to view the smallest possible angles accessible at the ISR. The solid angle and the laboratory angular range seen by each telescope are given in Table 1.

Each telescope was equipped with three multiwire proportional chambers (MWPC) of two planes each (total of 5000 wires). They provided the possibility of track reconstruction and therefore a very powerful method of screening background events. In addition, each telescope was equipped with a 5 cm thick Pilot 425 Čerenkov counter to tag fast particles. The counters of each telescope were equally spaced over a total flight path of 2 m, with the exception of telescope δ (1.5 m). The telescope counter sizes and spacings were finalized after experience gained in early test runs at the ISR. For example, we detected a considerable background of very soft γ-rays, which particularly limited the rejection power of a telescope close to the forward direction. Consequently, a tenth counter was added to the telescopes A and W, providing us with an additional dE/dx measurement.

Two large monitor counters (50×100 cm^2) U11 and U12, placed on top of the vacuum pipe, are shown in Fig. 3. Together with identical counters placed under the pipe, they formed the monitor counters R1 for Arm 1. Four identical counters were placed symmetrically on the outgoing Arm 2 (R2). These counters were used to optimize the beam-beam interaction rate and to monitor the luminosity of the colliding beams during the experimental runs. Small counter telescopes (BG1, BG2) symmetrically placed on the upstream sides of the beam intersection region proved extremely useful for monitoring the beam-gas and beam-wall background rates.

The experiment profited considerably from the installation of a special thin-walled vacuum chamber. The central bicone had a wall thickness of 0.3 mm, and the 6 m long downstream arm of ring 1 was fabricated from 0.15 mm corrugated stainless steel. Compared to a conventional pipe (2 mm thickness), the rate of background events (predominantly due to soft γ-showers) was reduced by almost a factor of 10; furthermore, the apparent multiplicity of the p-p events decreased considerably.

3. ELECTRONICS

3.1 Trigger conditions and trigger logic

We employed two main trigger conditions to select with high efficiency a class of events which would contain quarks, while rejecting particles with $|Q| = 1e$:

i) dE/dx trigger: In any one of the six telescopes it required a simultaneous energy loss in counters

$$C_1, C_2, C_3, C_4, C_6, C_7, C_8, C_9 > 0.04\ \varepsilon_0$$

and in $$C_2, C_4, C_5, C_6, C_7, C_8 \quad < 0.95\ \varepsilon_0\ .$$

Here and in the following discussion, ε_0 is the most probable energy loss ε_p of a min.I. particle. The low-level threshold permitted the efficient detection of relativistic $|Q| = 1/3e$ quarks (for which $\varepsilon_p = 0.10\ \varepsilon_0$ for our counters), yet rejected well the PM noise and very small energy deposits. The upper level requirement (veto levels) removed a very large fraction of min.I. particles from the trigger, but permitted efficient detection of $|Q| = 2/3e$ quarks with a velocity down to $\beta \sim 0.7$. Particles with charge in the range $0.3e < |Q| < 0.8e$, and more precisely the following classes of events, satisfy this trigger:

a) $|Q| = 1/3e$ quarks in the velocity range $0.35 < \beta < 1$;

b) $|Q| = 2/3e$ quarks in the velocity range $0.7 < \beta < 1$;

c) $|Q| = 1e$ min.I. particles, but only with a small probability, since there is a $\sim 0.01\%$ chance that the dE/dx losses are $< 0.95\ \varepsilon_0$ in the specific six counters (for our telescopes);

d) particles with $|Q| = 1e$ going through the PM's (which are tagged by the PM anticounters in pattern units, but not rejected on-line);

e) accidental edge events;

f) other background events (e.g. low-energy γ-showers, producing Compton and photoelectrons in the scintillators).

ii) Time-of-flight (TOF) trigger: In any one of the five telescopes (excluding L) it required $0.24 < \beta < 0.55$ and a simultaneous energy loss in counters

$$C_1, C_2, C_3, C_4, C_6, C_7, C_8, C_9 > 0.04\ \varepsilon_0\ .$$

All particles in this β-range were accepted irrespective of charge, provided their range was larger than ∿ 24 g cm^{-2} (the effective thickness of our telescopes). This requirement on the range $R = (M/Q^2) \cdot f(\beta)$ together with $\beta < 0.55$ implied that $M/Q^2 > 1$ (M_p/e^2), which effectively excluded protons from the trigger. The energy loss requirement of $> 0.04\ \varepsilon_0$ excluded the detection of particles with $|Q| < 0.1e$; pulse-height saturation of the PM's at $\sim 5\varepsilon_0$ excluded particles with $|Q| > 3/2e$.

The following classes of events are accepted:

a) $|Q| = 1/3e$ with $M > 0.11$ GeV/c^2,
$|Q| = 2/3e$ with $M > 0.44$ GeV/c^2, and
$|Q| = 4/3e$ with $M > 1.8$ GeV/c^2;

b) deuterons and heavier $|Q| = 1e$ particles;

c) nearly stopping protons;

d) accidentals simulating slow particles.

A block diagram of the trigger electronics for the two triggers is shown in Fig. 4. The PM anode signals of the quark counters went to fivefold linear fan-outs (LF). To form the low-threshold requirement for both triggers, one output (amplified by a factor of four) from each of the eight LF's from the appropriate telescope drove a shaper (S), set at a threshold of $0.04\ \varepsilon_0$. The outputs of the shapers were combined in an eightfold coincidence. For the upper-level discrimination of the dE/dx trigger, the outputs of the six corresponding LF's after attenuation (A) drove six updating discriminators (UDD) set at thresholds of $0.95\ \varepsilon_0$. Their outputs were OR-ed and used in anticoincidence with the output of the low-level eightfold coincidence to accomplish the dE/dx trigger requirement.

The β-requirement for the TOF trigger was realized with the use of a special output [linear overlap output (L O)] of an eightfold coincidence circuit (CERN Model N6135). This output had a pulse width determined by the temporal overlap of the first and last input pulse arriving at the coincidence; by appropriately staggering the inputs to the eightfold coincidence, this overlap was made longest for the slowest particles. This output and a prompt logic-level output of the eightfold coincidence were timed in the "TOF coincidence", such that a trigger was produced for all particles in the β-range $0.24 < \beta < 0.55$.

A telescope was gated off for 1 μsec, each time any of the six updating veto discriminators of that telescope gave a signal. This veto, while causing less than 5% dead-time, served the following purposes:

a) it eliminated, after a very large energy deposit, spurious afterpulses (reflections, ringing, etc.) of the counters which could simulate quark-like signals;

b) it ensured that the energy deposit recorded for each candidate was not masked by being superimposed on the tail of a preceding large pulse.

Each trigger initiated gates for the analog electronics, the MWPC's, and the subsequent read-out. An EMR 6130 computer was used for the data acquisition and on-line monitoring.

3.2 Analog signal electronics

A block diagram of the analog electronics used for the pulse-height registration is shown in Fig. 5. One output of each of the LF's was connected through delays to its appropriate linear gate (LG). A trigger signal (dE/dx or TOF trigger) of a certain telescope opened the corresponding nine gates. This permitted the multiplexing of the equivalent LG outputs of all six telescopes in linear mixers (LM), and one set of nine encoders was used to digitize the pulse-height information, which was read out via CAMAC scalers. The response of the system was linear for energy losses in the range $0.04\ \varepsilon_0 < dE/dx < 4.0\ \varepsilon_0$.

A further set of outputs of the nine LG's was sequentially delayed and then mixed in an LM. Its output was displayed on a Tektronix 7704 oscilloscope, equipped with an P-11 phosphor and operated at a sweep speed of 50 nsec cm^{-1}. This oscilloscope was viewed by a high-sensitivity TV camera, and connected to a commercial TV monitor which in turn was photographed with an automatic film camera. The sweep of the vidicon and hence the video signal was inhibited and initiated by the computer. During the "Inhibit" period the vidicon stored the picture information, while the on-line software decided, on the basis of simple pulse-height consistency requirements, whether the nine pulse heights of an event should be photographed or not. For picture-taking, the computer initiated the sweep of the TV Camera, which displayed the picture on a monitor; otherwise the vidicon was simply erased.

These pictures, reduced in rate from the trigger rate by a factor of $\sim 10^3$, were taken as a further aid in the analysis of possible candidates. They were also a valuable aid in the identification of background sources, such as the one associated with the tail of large PM pulses.

4. DETECTION CAPABILITIES, EFFICIENCY AND ACCEPTANCE OF THE DETECTOR

4.1 Simulation of the quark signals

The detection properties of the telescopes and their associated electronics, were studied in a test beam of the CERN PS, where both positive and negative pions in the momentum range 0.2-1.2 GeV/c and protons in the range 0.6-1.2 GeV/c could

be selected. Each counter of the test telescope, identical to telescope α, was equipped with four optical filters, which could be remotely inserted in various combinations between the light-guide and the PM of the counter. In this way the scintillation light could be attenuated up to a factor of 50, permitting a systematic investigation of the response of the electronics to a range of simulated low-energy losses. The electronics used were in all aspects (such as length of signal cables, timing, etc.) identical to the instrumentation used at the ISR experiment.

A Monte Carlo calculation provided detailed verification of these measurements. The heart of the calculation was a program to evaluate the energy loss distribution[19] (Vavilov distribution) with an expected validity from $\beta = 0.2$ and m_π up to the highest β's and masses kinematically allowed in our experiment. As an example, we verified that the energy loss distributions computed with this code correctly reproduce the measured mean energy loss[20] for π's and p's in the range $0.2 < \beta < 0.99$. Furthermore, it correctly reproduces the measured charge dependence of dE/dx for $|Q| \geq 1e$, and it agrees with the predictions at present accepted for $|Q| < 1e$; in particular, the most probable energy loss of a minimum ionizing $|Q| = 1/3e$ particle is $\sim 1/10$ the energy loss of a particle with $|Q| = 1e$ for our thickness of scintillator[21]. The density effect[22], an important correction to the energy loss of relativistic particles in solids, has the same Q^2 dependence as the average loss, and is correctly treated in the program.

In these Monte Carlo calculations relevant features of the apparatus could be considered, such as photoelectron yield, light filtering (for test beam measurements), light collection non-uniformity of the counters, etc. As an example of the agreement between calculation and measurement, we show in Fig. 6 the measured and computed energy loss distributions for a particular counter. This excellent agreement in all cases where measurements could be made, gave us confidence that the calculations could be extended to predict the response of our detector to exotic particles (with fractional charges and/or large masses).

4.2 Electronic efficiency

The efficiency of the eightfold coincidence as a function of energy loss and discriminator-level settings was also measured in the test beam. For a threshold setting corresponding to $0.04\ \varepsilon_0$, as was used throughout the experiment, we measured for a light output corresponding to a $\beta = 0.96$, $|Q| = 1/3e$ quark, an efficiency η of 0.96 ± 0.04. The error corresponds to a change of all discriminator levels by $\mp 0.01\ \varepsilon_0$ (∓ 10 mV).

Figure 7 shows the measured and computed results for the veto-level efficiency of $|Q| = 2/3e$ quarks as a function of β, which shows that charge 2/3e is efficiently detected for $\beta > 0.7$. The slight decrease in efficiency for $\beta \lesssim 1$ reflects the increase in the Landau tail of the dE/dx distributions. For $|Q| = 1/3e$ the veto discriminators limit the acceptance to $\beta > 0.35$.

The kinematically allowed momentum-mass range for particles produced in the reaction $pp \to pp\,q\bar{q}$ at 26.6 GeV/c on 26.6 GeV/c beam momenta is given in Fig. 8. (This is the energy at which the bulk of our data was taken.) The dE/dx trigger restricts the acceptance for $|Q| = 1/3e$ to above the line $\beta = 0.35$, whereas $|Q| = 2/3e$ is limited to above the line $\beta = 0.7$. A similar diagram, Fig. 9, shows the kinematical limits of the TOF trigger. The sensitive region lies between the lines $\beta = 0.55$ and $\beta = 0.24$. In addition, there was a range requirement ($R > 24$ g/cm^2), which was important for low mass particles.

4.3 Efficiency of the MWPC's

MWPC's were introduced for track reconstruction of possible slow ($\beta < 0.55$) particles, which are accepted by the TOF trigger. Since they could also be of value in the detection of minimum ionizing $|Q| = 1/3e$ and $|Q| = 2/3e$ particles, the detection efficiency of MWPC's for fractionally charged particles was carefully considered[23]. Based on measurements, which are in agreement with the theoretical understanding of the ion-pair collection mechanism, and on data on the influence of electronegative gas-admixtures on the electron collection process, the authors[23] arrive at a detection efficiency for min.I. $|Q| = 1/3e$ particles in excess of $\sim$ 75% per MWPC plane. In addition, we measured that these chambers were better than 99.95% efficient for normal minimum ionizing particles.

4.4 Acceptance calculations

Past quark searches at accelerators were carried out at production angles close to zero degrees in the laboratory system[9,10]. Kinematical effects are dominant, and consequently for "reasonable" quark production models the interpretation of these searches is insensitive to the exact knowledge of the quark angular and momentum distribution. At the ISR however, where laboratory and centre-of-mass systems are almost identical, the acceptance of an apparatus depends critically on the angular distribution of the particles to be detected.

Our detector acceptance was calculated using the quark production mechanism

$$pp \to pp + q\bar{q}$$

and two different assumptions about the differential cross section:

i) In the first model, we assumed isotropic production of quarks with kinematics imposed by four-body phase space;

ii) and in a second model[24] the transverse components of the momentum of the reaction products were restricted to follow a Gaussian distribution with $\langle p_T \rangle = 0.4$ GeV/c, as in typical hadronic collisions.

The results of these calculations are shown in Figs. 10 and 11.

For both models, which might represent two extremes of any quark production process, the mass acceptance is rather flat up to the highest possible masses. For isotropic production the acceptance is $\sim$ 1%; for the forward-peaked models it is close to $\sim$ 10%.

4.5 Summary of detection capabilities

The layout of the telescopes was optimized to assure efficient detection of quarks produced under a wide variety of production mechanisms:

i) Quarks could be detected in events having a very high hadron multiplicity. Since the six telescopes were electronically independent, the presence of normal particles in one telescope did not hinder the detection of quarks in any other telescope. Furthermore, even at the multiplicities observed at the highest ISR energies, only about 10% of the inelastic interactions gave one, and fewer than 0.4% gave more than one particle in any given telescope. Therefore, quarks produced in events of even much higher multiplicity would very likely be unaccompanied in a telescope by a second particle, and hence would be efficiently detected. (In Section 8 we estimate the highest multiplicity final state in which we could efficiently detect a quark).

ii) Apart from the pulse-height requirement, there was no other restriction on the trigger to limit the types of final states in which we could detect quarks. To provide this inclusive trigger, no additional counters which would ensure counting only beam-beam interactions (e.g. our R1 and R2 monitor counters) must be required in the trigger. However, under usual running conditions, background not associated with beam-beam interactions (beam-gas or beam-wall collisions) constituted less than 50% of the total triggers.

iii) Quarks produced at exactly 0° in the centre-of-mass system could be detected in this experiment. The 15° crossing angle of the ISR beam pipe has the effect that non-relativistic particles produced at 0° have a non-zero lab. angle and hence may leave the vacuum pipe. As an example, a 10 GeV/c^2 quark produced at exactly 0° with a momentum between 3 GeV/c and 6 GeV/c, or between 9 GeV/c and 18 GeV/c, would fall within the acceptance of the telescopes.

iv) Quarks produced with a very large transverse momentum could be detected, primarily with telescopes δ and L, which sample large production angles.

v) In contrast to most previous accelerator searches, no momentum-defining magnets were used. Consequently, this quark search was sensitive not only over a wide angular range, but also over a large range of momenta. For example, a 10 GeV/c^2 quark with charge 1/3e having a momentum anywhere between 2.5 GeV/c and 23 GeV/c would satisfy our trigger conditions. Furthermore, the detector was therefore sensitive to both signs of the charge.

5. DATA TAKING

5.1 Beam monitoring

For each running period (10-40 hours) the beam-beam (BB) collision rate was optimized while minimizing the beam-gas (BG) rates. Frequent measurements of the luminosity calibrated our BB monitors. The luminosity L can be expressed in the form

$$L = \frac{I_1 \cdot I_2}{e^2 \cdot c} \cdot \frac{1}{\operatorname{tg} \alpha/2} \cdot \frac{1}{h} ,$$

where I_1 and I_2 are the currents of the two beams, α is the crossing angle (15° at the ISR), and h is the effective vertical dimension of the beams. We measured the luminosity by displacing the two beams vertically, according to the method of Van der Meer[25], who pointed out that h can be deduced by measuring the BB collision rate as a function of the relative vertical separation of the two beams. During these beam displacements the coincidence rates of all telescopes were recorded, and from these the particle fluxes due to beam-beam and beam-gas interactions through each of the telescopes were determined.

5.2 Data taking

The following checks were carried out during data-taking periods:

i) Thresholds of all upper-and lower-level discriminators were monitored continuously and maintained to $\pm 0.01\ \varepsilon_0$ of the nominal settings (±10 mV in threshold voltage).

ii) Rates of all telescope coincidences, trigger rates, BB and BG rates were monitored continuously and compared for consecutive 15 min. time intervals.

iii) Every three hours the gains of all linear channels and the channels corresponding to zero pulse height were calibrated against the energy loss of min.I. particles. Any drifts were compensated with an adjustment of the PM high voltages, a procedure which kept gains constant to better than ±5%.

iv) Once per run, all TOF channels were calibrated to ±0.25 nsec.

v) The efficiency of the MWPC's was measured and wiremaps taken once per run.

For each trigger the following information was recorded on magnetic tape:

i) the nine dE/dx measurements for the telescope in which the trigger occurred;

ii) seven TOF measurements within the appropriate telescope, as well as TOF measurements of the BB monitors relative to the trigger time;

iii) the pulse-height in the appropriate Čerenkov counter;

iv) the complete MWPC information;

v) the rates of the R1 and R2 monitors during a 300 μsec interval, immediately following the trigger;

vi) the number of counts in R1, R2, BG1, BG2, and all of the telescopes since the previous event;

vii) the status bits of the pattern units in which are indicated trigger type and triggered telescope; which of the quark counters registered a pulse-height $dE/dx > 0.04\ \varepsilon_0$; which of the counters in the dE/dx veto registered a pulse height $dE/dx > 0.95\ \varepsilon_0$; which of the anticounters and monitor counters registered a pulse height $dE/dx > 0.08\ \varepsilon_0$.

6. ANALYSIS OF THE DATA

Different analysis procedures were required for the dE/dx and TOF trigger data, which are therefore treated independently.

6.1 Analysis of the dE/dx triggers

6.1.1 Preliminary cuts on the dE/dx triggers

The following preliminary cuts were applied to all data of the dE/dx trigger ($\sim 3.9 \times 10^6$ events):

i) Average energy loss, $\langle dE/dx \rangle$, less than $0.80\ \varepsilon_0$. This removed essentially all events associated with min.I. $|Q| = 1e$ particles. However, particles with charge $|Q| \leq 0.7e$ are efficiently accepted in the β-range $0.7 < \beta < 1.0$ (1.4×10^6 events removed).

ii) No signal in the anticounters protecting the PM's of the telescope in question. This requirement suppressed a major source of background due to the generation of Cerenkov light in the PM glass envelopes (0.4×10^6 events removed).

iii) Events were rejected which occurred during short (1 to 100 msec) periods of abnormally high background conditions of either of the two ISR rings. This cut was imposed to exclude the effects of momentary PM gain shifts observed, and to eliminate the somewhat increased number of accidental events recorded during such background bursts. The cut was based on the measured average rates in the monitor counters R1 and R2, and on the "instantaneous" rates recorded during a 300 μsec interval immediately following each event. This cut, which introduced an effective dead-time of $\sim$ 2%, removed 0.2×10^6 events.

After the cuts we were left with 1.9×10^6 events. The remaining effort in the analysis was directed towards finding and applying a test to this set of events which would best discriminate between the enormous background and any possible quark signal. The test finally adopted is based on the likelihood distribution, and is described in the following section. A further criterion was provided by a χ^2 test on the recorded TOF values (Section 6.1.3).

6.1.2 *Application and validity of the likelihood test for the energy loss in the counters*

To interpret the measured pulse heights for any given event in terms of the particle charge, we computed energy loss distributions (Section 4.1) as a function of Q and β of particles traversing the different counters of the six telescopes. Account was taken of various experimental parameters, such as geometry of the scintillators and photocathode statistics. For computational convenience each distribution was truncated, neglecting the low- and high-energy losses corresponding to an integral probability of 10^{-4}. The resulting energy loss probability distribution was normalized to one and divided into 100 equally spaced energy loss bins. The binned distributions $P_i^j(Q,\beta,\Delta E_k^j)$ measure the probability for a particle with charge Q and velocity β to suffer in the j^{th} counter of the i^{th} telescope an energy loss falling in the k^{th} bin ΔE_k. The likelihood $\mathscr{L}$ that the nine measured energy losses of an event are produced by such a particle is defined as

$$\mathscr{L}(Q,\beta) = \prod_{j=1}^{9} p_i^j(Q,\beta,\Delta E_k^j) \ .$$

Once the distribution of the $\mathscr{L}(Q,\beta)$ values is known for particles with a fixed Q and β, a lower limit on the value of $\mathscr{L}$ can serve as an acceptance criterion with known efficiency for these particles.

In a comparison between computed $\mathscr{L}$-distributions and those obtained for actual events, any possible correlations in these energy loss measurements in consecutive counters have to be considered. Such a correlation could be introduced, for example, through the creation of energetic knock-on electrons. An upper limit for this latter effect was computed by considering the asymmetric contribution to the high-energy tail of the dE/dx distributions as a probability measure for transferring the energy to a single energetic knock-on electron. These electrons were then tracked through the telescope. Even this overestimate caused only small changes in the distributions P_i^j and $\mathscr{L}$. For relativistic $|Q| = 1/3e$ quarks we calculated a 6% increase in the width of the $\mathscr{L}$-distribution; the efficiency for quark acceptance for a given $\mathscr{L}$-value changed by less than 5%. The trend of these changes proved to be consistent with experimental results, obtained from calibration runs at the ISR. In practice, calculations and comparisons were based on the natural logarithm of the likelihood function.

In Fig. 12 the Monte Carlo calculation of the $\ln\mathscr{L}$-distribution for $\beta = 0.96$ pions is compared with that measured for minimum ionizing particles at the ISR. Figure 13 shows the results of a similar calculation for $|Q| = 1/3e$, $\beta = 0.96$ particles, together with an experimental distribution (using filters) measured in the PS test beam, again showing close agreement between the measured and calculated

distributions. Since the light filter does not exactly simulate a fractionally charged particle, the two distributions are not expected to be identical, but the difference would be too small to be seen in this figure. As a result of the chosen normalization of the P_i^j-distributions, the position and width of the $\ln \mathscr{L}$-distributions are nearly independent of Q and β, and consequently the $\ln \mathscr{L}$ cut-off for a specified efficiency is almost independent of Q and β. The criterion $\ln \mathscr{L} > (-38.0)$ accepts particles of any Q or β with an efficiency of approximately 95% or greater.

6.1.3 Use of TOF measurements

For each event seven TOF measurements were recorded. This information could be used to distinguish between slow $|Q| = 2/3e$ quarks and $|Q| = 1e$ min.I. particles, and as a possible further means of background rejection. For this purpose the TOF distributions were studied in the test beam systematically as a function of pulse height. For min.I. $|Q| = 1e$ particles they were identical to the distributions obtained from calibration runs at the ISR. In Fig. 14 the measured standard deviations σ_i of the inverse velocity distributions

$$\beta_i^{-1} = \frac{0.3 \times \mathrm{TOF}_i}{d_i} \left[\frac{\mathrm{nsec}}{\mathrm{m}}\right]$$

are plotted as a function of ε_p, the most probable energy loss, where TOF_i and d_i are the flight times and distances, respectively, between counters 1 and i. (The quantity β^{-1} is used because it is proportional to TOF, and its distribution is Gaussian).

Since for $\varepsilon_p \sim 0.1\ \varepsilon_0$, the σ_i's are strongly pulse-height dependent, we chose for the TOF analysis of possible relativistic $|Q| = 1/3e$ quarks the σ_i's corresponding to $\varepsilon_p = 0.065\ \varepsilon_0$. This ensures a well-defined lower bound for the efficiency of a cut on $\chi^2(\langle\beta^{-1}\rangle)$, where

$$\chi^2(\langle\beta^{-1}\rangle) = \sum_{i=1}^{7} \frac{(\beta_i^{-1} - \langle\beta^{-1}\rangle)^2}{\sigma_i^2} \quad .$$

6.1.4 Results of the analysis of Set I

The procedure and the results of the following analysis are valid for all particles accepted by the dE/dx trigger, independent of their charge and velocity. However, to simplify the analysis, the data were arbitrarily divided into two sets on the basis of the energy loss for each event. Those with small energy loss were put into Set I, and those with higher but still sub-minimum-ionizing energy loss were put into Set II, as described below.

Before applying the likelihood test to the data, we screened all 1.9×10^6 events with an "Upper-Bound Likelihood" criterion ($\mathscr{L}_{ub}$) as follows:

i) We calculated ε_p for each event by using the average of those six out of the nine dE/dx measurements which are most tightly clustered (i.e. those six dE/dx values resulting in the smallest σ of the distribution). If $\varepsilon_p \leq 0.42\ \varepsilon_0$, the event was put into Set I ($\sim 2.1 \times 10^5$ events); we emphasize that the value of 0.42 is arbitrary.

ii) We computed a scaling factor $F = 0.1/\varepsilon_p$, from which scaled values $(\widetilde{dE/dx})_j = F(dE/dx)_j$ are computed. This permits the comparison of the scaled energy losses of an event with the P_i^j distributions for relativistic $|Q| = 1/3e$ quarks, for which $\varepsilon_p = 0.1\ \varepsilon_0$.

iii) We used the distributions $P_i^j\ (Q = 1/3e,\ \beta = 0.98,\ \Delta E_k^j)$ for the particular telescope to arrive at an Upper-Bound Likelihood" estimate, defined as:

$$\mathcal{L}_{ub} = \prod_{j=1}^{9} P_i^j(Q = 1/3e,\ \beta = 0.98,\ \Delta E_k^j)\ .$$

Since the dE/dx distribution for $|Q| = 1/3e$, $\beta = 0.98$ quarks is relatively wider than for any other particles of any $|Q| > 1/3e$ and any $\beta \leq 0.98$, this procedure gives an estimate of $\mathcal{L}$ which is too optimistic for $|Q| > 1/3e$ particles, i.e. $\mathcal{L}_{ub} \geq \mathcal{L}$. For example, a requirement of $\ln \mathcal{L}_{ub} > (-38.0)$ accepts relativistic $|Q| = 1/3e$ quarks with 95% efficiency, but is more efficient for $|Q| > 1/3e$ with $\beta \leq 0.98$. The validity of all steps of this test was verified with Monte Carlo calculations (e.g. computation of ε_p, increase of efficiency for scaled energy losses for $|Q| > 1/3e$, $\beta \leq 0.98$).

In Fig. 15 we show the distribution of $\ln \mathcal{L}_{ub}$ for all our data with $\varepsilon_p \leq 0.42\ \varepsilon_0$. Only 27 of the 2.1×10^5 events pass our minimal 95% efficiency criterion $\ln \mathcal{L}_{ub} > (-38.0)$, indicating the fact that the vast majority of our candidates had highly inconsistent energy losses.

In a second step these 27 events were tested against dE/dx distributions for $\beta = 0.98$ particles with charge Q' so that the ε_p of these distributions was the same as the measured ε_p for the event. (This again is too optimistic, for particles with $\beta < 0.98$ and a correspondingly smaller Q'.) Eight of the 27 events survived the cut-off at (-38.0) using this improved $\ln \mathcal{L}$ estimate. To these events a TOF cut $\chi^2((\beta^{-1})) \leq 12.5$ ($n_D = 6$) was applied. This cut is at least 95% efficient, since the σ's corresponding to $\varepsilon_p = 0.065\ \varepsilon_0$ were used. One event remains and its signature is given in Table 2. Before discussing the significance of this event, we report the results for data with $\varepsilon_p > 0.42\ \varepsilon_0$ (Set II).

6.1.5 Results of the analysis of Set II

All events with $\varepsilon_p > 0.42\ \varepsilon_0$ (computed as explained in the preceding section) were screened with an analogous procedure:

i) We computed a scaling factor $F = 0.42/\varepsilon_p$, with which the scaled energy losses $(\widetilde{dE/dx})_j = F(dE/dx)_j$ were computed.

ii) We used the relativistic distributions $P_i^j(Q = 2/3e, \beta = 0.98, \Delta E_k^j)$ for which $\varepsilon_p = 0.42\ \varepsilon_0$ to compute the $\mathscr{L}_{ub}$ estimate.

Again, this is strictly correct only for $|Q| = 2/3e$, $\beta = 0.98$ particles, and gives $\mathscr{L}_{ub} \geq \mathscr{L}$ for other particles with $|Q| \geq 2/3e$, $\beta \leq 0.98$. The result for all our data of Set II is shown in Fig. 16.

Of all the events with $\varepsilon_p > 0.75\ \varepsilon_0$, 66 candidates have a $\ln \mathscr{L}_{ub} > (-38.0)$, but not a single event has a $\langle \beta^{-1} \rangle \geq 1.25$ (corresponding to $\langle \beta \rangle \leq 0.8$) and a $\chi^2(\beta^{-1}) \leq 15.0$, which would correspond to a slow particle with charge in the range $1/3e \leq |Q| \leq 2/3e$. These events are, in the majority, accidental coincidences of several $|Q| = 1e$ particles going through the edges of the counters, consistent with their signature in the MWPC's.

In the group of events with $0.42\ \varepsilon_0 \leq \varepsilon_p \leq 0.75\ \varepsilon_0$, there are four events with $\ln \mathscr{L}_{ub} > (-38.0)$, of which three survive the test with the improved distribution. Again, these are accidental events as indicated by the very high $\chi^2(\langle \beta^{-1} \rangle)$, which for the three events is 13183, 412 and 25 respectively. The uniformity of the pulse heights and consequently the extremely high $\ln \mathscr{L}$-value of these three events reflects the bias introduced by our upper level discriminators. We conclude that we have no candidates in Set II, which implies for example no candidate of $|Q| = 2/3e$ and $0.7 \leq \beta \leq 1.0$.

6.1.6 Discussion of candidate

To understand the significance of our candidate in Set I, we studied the dependence of the distribution of $\mathscr{L}_{ub}$ on various parameters. Figure 17 shows the $\ln \mathscr{L}_{ub}$ estimate for a portion of the data together with that for those events having $\chi^2(\langle \beta^{-1} \rangle) < 12.5$. No significant difference in the distribution can be seen in comparing events with good and poor timing.

In Fig. 18 the $\chi^2(\langle \beta^{-1} \rangle)$ distribution is shown for two quite different ranges of ε_p for about 15% of our data. Again, no significant difference is seen among these χ^2 distributions. The relative flatness of the distributions is consistent with the hypothesis that the dominant source of our background is low-energy γ-showers. Very likely, several γ-rays interact in each counter of the telescope, randomly distributed over the active area of the scintillator.

Further information which can be brought to bear on the interpretation of the candidate is given below:

i) Signal in the large monitor counters

In a large fraction of our data we have looked for a possible correlation between $\ln \mathscr{L}_{ub}$-distributions and the signal in the monitor counters along Ring 1 and Ring 2 recorded for each event. No such dependence was found. In particular, the one remaining event is consistent with either a beam-beam or a beam-gas event

along Ring 1. About 70% of our events show precisely this signature. Our candidate is therefore not distinguishable from background on the basis of the monitor counter information.

ii) Number of counters in the telescope

We have re-analysed our data using successively six, seven, or eight counters of a telescope for the pulse-height information, and have looked for inconsistent changes in the number of candidates. No such inconsistencies were found.

iii) Associated particles in other counters

It is characteristic of our background events that a large number of neighbouring counters are usually struck in a random way and with energy loss less than ε_0. In particular, events in a small-angle telescope almost always show many of the counters and many tens of wires in the other small-angle telescope hit. This is consistent with the γ-shower hypothesis, according to which our low pulse-height trigger selects soft γ's and requires the more energetic electrons of the shower to go in a different direction. A similar pattern is observed in the intermediate angle system. Our candidate shows this characteristic signature, and from this point of view is again consistent with background events.

iv) Clusters in the MWPC's

For our candidate we find in the six MWPC planes only one possible cluster which could be associated with a straight track originating from the interaction region and going through the telescope. Taking the very pessimistic estimate of 50% for the detection efficiency for relativistic quarks in each gap, about 90% of all quarks would fire more than one gap.

On the basis of all these considerations we believe that our candidate is not a quark. From this result we can say that we have seen no $|Q| = 1/3e$ quarks with $0.35 < \beta < 1.0$ and no $|Q| = 2/3e$ quarks with $0.7 < \beta < 1.0$. A similar statement can be made for quarks of any charge between 0.3e and 0.8e, with a mininum β which depends on the charge.

6.2 Analysis of the TOF trigger

As indicated earlier, the nature of the events satisfying the TOF trigger required an analysis technique differing from those employed in the dE/dx trigger. The main differences are the following:

i) The large dE/dx for quarks with low β allowed efficient detection of these particles in the MWPC's, and made track reconstruction useful for screening events.

ii) The energy loss distributions in our counters for quarks with low β are approximately Gaussian, which means that a simple χ^2 test could replace the likelihood test used in analysing the dE/dx trigger.

iii) We had to take into account the possibility that the particles could slow down or stop in the detector. This turned out to be complicated, since these effects depend on the mass of the particle as well as on Q and β, and certain approximations were made, but at each stage the efficiency of the cuts used could be tested on Monte-Carlo-generated events.

6.2.1 Preliminary cuts for TOF trigger

The following computer cuts were applied to the total recorded number of 4.0×10^6 TOF triggers:

i) No signal in either of the anticounters in the triggered telescope. Most of the 2.4×10^6 events eliminated by this cut were due to relatively fast particles slanting away from the PM's and thus simulating a slower particle, which was accepted by the trigger.

ii) One track only through the triggered telescope, originating from the interaction region; essentially all of the 1.1×10^6 events rejected by this cut were accidental coincidences between two fast particles. Based on a Monte Carlo calculation of multiple scattering, the goodness-of-fit criterion in the track-finding program was chosen to ensure a reconstruction efficiency greater than 95%.

iii) As with the dE/dx triggers, no events were accepted which occurred during short periods of abnormally high background conditions (1.2×10^4 events eliminated).

After these cuts 0.5×10^6 events remained. For these events χ^2's for the energy loss and TOF measurements were calculated and cuts were applied, as described below.

6.2.2 Consistency of the energy loss measurements

For our counter thickness and for most of the mass and velocity range for which the TOF trigger is sensitive, the energy-loss distribution is well approximated by a Gaussian, and in fact for a given charge the width σ of this distribution is almost independent of β [21]. For example, for $|Q| = 2/3e$ particles, the width σ varies between 0.28 and 0.31 MeV in the β-range $0.25 \leq \beta \leq 0.55$ within our counters. If this were the only effect, a χ^2 for the energy loss measurements could be simply calculated for each event.

However, for many quarks which would be accepted by this trigger, and certainly for the slow protons and deuterons which were accepted, the particles could be expected to slow down, or indeed stop in the last counter of the telescope, leading to an

energy loss which increased from counter to counter. This effect depends not only on Q and β, but on the mass of the particle as well. Furthermore, the effect is non-linear, and straggling introduces correlations among the energy losses, so that an accurate fit to the expected distributions becomes unfeasible.

Therefore, we decided to use a linear fit to approximate the expected measurements and to determine the efficiency of any cuts which depend on M and β on a suitable sample of Monte-Carlo-generated events.

The method chosen was to perform a least-squares fit of the nine measured energy losses ΔE_i to the linear form

$$\widetilde{\Delta E}_i = \widetilde{\Delta E}_5 + T_i \Delta\varepsilon \ .$$

The parameters to be determined are $\widetilde{\Delta E}_5$ and $\Delta\varepsilon$, which are the energy loss in the reference counter C_5 and the incremental energy loss per unit of counter thickness; T_i is the thickness between C_i and C_5 (T_i in g cm^{-2}). Then the χ^2 estimate of the goodness-of-fit was formed:

$$\chi^2(\Delta E) = \sum_{i=1}^{9} \left(\frac{\Delta E_i - \widetilde{\Delta E}_i}{\sigma_i} \right)^2 \ .$$

For a particle which slows down only slightly or not at all, this χ^2 should be distributed like a theoretical χ^2 distribution for 7 degrees of freedom, but for a particle which slows down appreciably, or stops, the distribution will be shifted to somewhat higher values of χ^2.

6.2.3 Consistency of the TOF measurements

The problem of particles which slow down is less severe for the measurement of β for two reasons: i) the dependence of the effect on β is less strong than that for the energy loss; and ii) the TOF measurements give β averaged over the flight path, further decreasing the variation. Here it was found sufficient to fit the measured TOF's to a single $\langle \beta^{-1} \rangle$ as described in Section 6.1.3, yielding for each event a weighted average $\langle \beta^{-1} \rangle$ and a

$$\chi^2(\langle \beta^{-1} \rangle) = \sum_{i=1}^{7} \left(\frac{\beta_i^{-1} - \langle \beta^{-1} \rangle}{\sigma_i} \right)^2 \ .$$

Here the σ_i are chosen on the basis of the errors in the TOF measurements.

6.2.4 Monte Carlo simulation for the TOF trigger

A Monte Carlo program tracked particles with charge $|Q|$ = 1/3e, 2/3e and 1e through the telescopes, computed the energy loss in each counter, and the corresponding TOF's between counters.

The average energy loss of particles with given Q, M and β was obtained by interpolation of tabulated range-energy relations[20]. In each counter the energy loss was randomized according to a Gaussian distribution with a fixed width taken to be the average width in the β-range accepted by the trigger. After each counter, β was recalculated and this new β was used to calculate the average energy loss in the following counter. The sequence of β's obtained in this way were converted into TOF's and randomized using the known time resolution of the apparatus.

To allow a direct comparison, we corrected the measured energy losses and TOF's in the real data for effects which depended on the position of the track in the counters. The corrections, which were typically one nsec for the TOF's, and 10% for the energy losses, were determined using calibration runs with minimum ionizing particles.

One example of the validity of these calculations is shown in Fig. 19, where the measured average energy loss of slow protons ($0.57 \leq \beta \leq 0.65$) is compared with the computed energy loss in the nine counters of a telescope. In the calculation, protons with a β spectrum identical to the recorded sample were used. The agreement between measured and calculated average energy losses is excellent, and the increase in dE/dx from the first to the ninth counter, due to the slowing down of the protons, provides an independent check on the β measurement with a sensitivity of better than ±5%. The data bars give the width 2σ of the dE/dx distributions. They increase towards the ninth counter, owing to the β-range of protons accepted. Again good agreement is found except for the last counters in a telescope, where the measured widths exceed the theoretically expected ones. As mentioned previously, the TOF trigger preferentially accepted protons which slanted away from the PM's and went through the ends of the counters. This amplified the effect of non-uniformity of the light collection in the large scintillators and is responsible for the increased widths in the distributions.

These experimentally determined σ's were used in the subsequent analysis of the TOF data.

6.2.5 Determination of the χ^2 cuts

From our previous discussion, it is clear that the efficiency of a χ^2 cut will in general depend on β and M. As an example, we show in Fig. 20 the $\chi^2(\Delta E)$ distribution for protons as measured and as calculated for a Monte Carlo sample of protons with the same velocity spectrum as that of our data. With this Monte Carlo program, Table 3 was computed giving the combined χ^2-cut efficiency as a function of β and M for $|Q| = 2/3e$ particles as was used for the analysis. A similar table was derived to evaluate the analysis efficiency for $|Q| = 1/3e$ particles.

6.2.6 Results of the TOF - Trigger Analysis

After cuts in $\chi^2(\Delta E)$ and $\chi^2((\beta^{-1}))$ were applied to the data, a large number of events remained, which were mainly slow protons and deuterons, the latter probably

produced in the walls of the ISR vacuum chamber. The events with poor χ^2 values were due to accidental reconstructions in the MWPC's, and to particles interacting in the telescope so as to simulate a slow particle.

From the average energy loss and β of each remaining event, an effective $|Q|$ was computed. In Fig. 21 we summarize all our TOF data, after application of the χ^2 cuts. The large peak at $|Q| = 1e$ is due to protons and deuterons with a tail down to a value of $|Q| = 0.85e$. We also show the expected Q distribution for $|Q| = 2/3e$ quarks with mass $M = 10$ GeV/c^2 and velocities β in the range $0.3 \leq \beta \leq 0.55$.

Although the analysis was illustrated for $|Q| = 2/3e$ quarks, the results apply to quarks with charge less than 2/3e and, in fact, those with slightly greater charge.

Since we have no candidate within the 90% confidence band, we can say that we have found no quark candidate with charge in the range $0.1e < |Q| < 0.8e$ among our TOF trigger data.

7. FLUX AND CROSS-SECTION LIMITS

Table 4 shows the luminosity, integrated over the total running time, for each of the three s-values at which data were taken. These numbers are accurate to better than 10%.

In Table 5 we have summarized our results in terms of flux limits (90% confidence level) of quarks through the six telescopes, again integrated over our total running time. Combining the data of all three energies we find that the quark flux is less than $\sim 6 \times 10^{-10}$ of the normal particle flux at the ISR.

In the measurement of the flux of normal particles, the total number of observed events had to be corrected for the contribution of particles not associated with primary beam-beam interactions. This correction was obtained by determining the fraction of tracks not originating in the interaction region and, secondly, by measuring the dependence of the telescope rates on the rate of beam-beam collisions during the luminosity measurements (Section 5.1). The fluxes derived by this method had an error of less than ±10%.

As in our previously reported work[18], we have derived cross-section limits, assuming as the quark production reaction

$$pp \rightarrow pp + q\bar{q}$$

While this reaction serves as a convenient calculational example and is a way of making a comparison with other searches, our primary result is the flux limit, which is completely independent of a particular production mechanism or of the angular distribution assumed in a model.

The cross-section calculations follow the assumptions made for the acceptance calculations (Section 5.4). Here we state only our results for the restricted phase-space model and show in Figs. 22 and 23 our final cross-section limits together with our previous results. The substantial improvement is due partly to the longer running time and partly to the analysis of the TOF trigger data. These graphs represent our results for ISR operation at $s = 2830$ GeV^2 only. Results based on our data for $s = 2080$ GeV^2 and $s = 3844$ GeV^2 can be inferred from Table 5. Although our total luminosity at $s = 3844$ GeV^2 was relatively small, our sensitivity for quark masses up to ~ 30 GeV/c^2 is estimated to improve the present cross-section limit from cosmic-ray experiments by about a factor of 10.

Recently, results from other searches for heavy stable particles at the ISR were reported[26,27]. No particles with charges $|Q| \leq 2e$ were found at an estimated cross-section limit of $\sigma \approx 10^{-32}$ cm^2 (90% confidence). From the results obtained in the first reported search at FNAL[17], the authors consider it "unlikely that the production cross-section of either charge $|Q| = 1/3e$ or $2/3e$ is greater than 10^{-35} cm^2". In this search the kinematical mass limit was about 12 GeV/c^2. In another, more recent and more sensitive search at FNAL, again no evidence for quarks was found[28]. Based on a production model with limited transverse momentum, cross-section limits for charge $Q = -1/3e$ between 10^{-38} and 10^{-39} cm^2 for quark masses up to 8.5 GeV/c^2, and for charge $Q = -2/3e$ between 10^{-37} and 10^{-38} cm^2 and quark masses up to 10.5 GeV/c^2 were quoted. Since this search was sensitive in a rather restricted kinematic range ($p_T \approx 0$ and $x \gtrsim 0.5$ for the quarks, typically) the above cross-section limits increase by three orders of magnitude, if the calculations are based on an isotropic production model. Cross-section limits for the positively charged quarks are a factor of 100 higher.

8. DISCUSSION AND CONCLUSION

In this section we summarize the important features of this quark search and indicate possible limitations which might have interfered with the detection of quarks.

8.1 Upper and lower limits of mass acceptance

For the s-value, $s = 2830$ GeV^2, at which the bulk of our data was taken, the kinematical mass limit for pair production in the reaction $pp \to pp + q\bar{q}$ is $M = 25.4$ GeV/c^2. It is only slightly larger than the highest mass quark which we could have detected from this reaction, $M = 24.6$ GeV/c^2.

Another reaction $pp \to p + p\bar{q} + q$ is imaginable, in which quarks with masses $M > 25.4$ GeV/c^2 could be produced, assuming that the mass of the bound $p\bar{q}$ system

is correspondingly small. In this model, our detector could in principle have detected quarks with masses as high as ~ 47 GeV^2/c. Obviously, the detection of the $p\bar{q}$ system would have also been possible.

Recently, nucleon models became increasingly popular, in which the constituents are thought to be much lighter than the nucleon, which in turn necessitates the invention of various mechanisms to explain the absence of free quarks[29]. Alternatively, such very light quarks might only be knocked out of the potential well if a very high transverse momentum p_T is transferred to it in the hadron-hadron collision[30]. Such high p_T processes would not have been observed in any of the previous accelerator searches, where the quarks were always looked for at production angles close to 0°. However, in this experiment the whole range of production angles from 0° to 90° was covered; the dE/dx trigger was uniformly sensitive down to masses $M \approx m_e$, the electron mass; the TOF trigger gave sensitivity down to $M = 0.10$ GeV/c^2 for $|Q| = 1/3e$ particles and $M = 0.42$ GeV/c^2 for $|Q| = 2/3e$ particles, respectively.

8.2 Multiplicity limits

It was previously emphasized that the layout of the quark telescopes was optimized for detecting quarks amongst a wide variety of final states: our trigger was truly inclusive; our acceptance in mass and momentum, was essentially limited only by kinematics.

Even so, any quark which was accompanied by a normal charged particle in the same telescope would not have been detected by us. This limitation becomes most serious for quarks produced in events with high multiplicity, and its effect can be estimated as follows.

For the high-multiplicity events we assume the same angular (rapidity) distribution as that observed for typical events at ISR energies. Secondly, we assume Poisson statistics for finding n particles per event in a given telescope. With these assumptions we estimate a 50% detection efficiency for charged multiplicities as high as ~ 150 in the most unfavourable telescope (computed for $s = 2830$ GeV^2).

What happens to our detection efficiency for quarks produced together with a "jet" of other particles? In this case the kinematical differences between centre-of-mass and laboratory system will frequently destroy a tight spatial correlation and allow the detection of the quark. For example, if a quark is produced very close to 0° with a velocity $\beta \leq 0.9$, it will leave the vacuum pipe (as described in Section 5.5.3) and be detected, whereas an accompanying jet of relativistic pions will stay very close to the forward direction and will not obscure the detection of quarks.

Could we have seen relativistic quarks which stayed inside an accompanying jet? To estimate the efficiency for this mechanism, we used a parton fragmentation picture, the fragments having a flat rapidity distribution along the original parton direction and a limited transverse momentum. This model predicts even for a jet multiplicity as high as 8, a geometrical efficiency close to 100% (i.e. the quark is almost always unaccompanied in the telescope and no particles hit the anti-counters). Only in telescope L (which subtends a large solid angle) is the efficiency lowered to $\sim$ 10%.

9. ACKNOWLEDGEMENTS

This experiment owed much to our close association with Dr. B. Hyams; his concern, advice, and support were greatly appreciated. We are grateful for many important contributions by Dr. M. Bott-Bodenhausen throughout the course of the experiment. We acknowledge with pleasure the continued interest of Dr. G. Charpak and Professor J. Steinberger who both suggested the experiment to some of us. The merits of placing the telescopes in the beam plane were first pointed out to us by Professor A. Zichichi. We thank Dr. K. Winter, with whom we combined efforts to obtain the thin-walled vacuum chamber. We are grateful for generous aid received from Dr. A. Minten and the other members of the SFMD group. Our technicians contributed with skillful work. At all stages of the experiment we benefitted from the support of the ISR Department, from its Experimental Support and Vacuum Group and from the assistance of the ISR Coordinator.

Table 1

Geometrical parameters of the quark telescopes

Telescope	Central angle (degrees)	Angular range (mrad)	Solid angle (msr)
A	0.9	9- 24	0.36
W	2.4	20- 62	0.46
α	7.8	104- 170	5.4
β	12.7	190- 255	4.6
δ	27.1	390- 555	8.6
L	67.7	1040-1330	22.8

Table 2

Signature of the candidate in the Set I data

Telescope	ε_P $[\varepsilon_0]$	$\left\langle \frac{dE}{dx} \right\rangle$ $[\varepsilon_0]$	$\ln \mathscr{L}$	$\langle \beta^{-1} \rangle$	$\chi^2(\langle \beta^{-1} \rangle)$
β	0.12	0.15	-32.2	1.1	2.6

Table 3

Efficiency for the combined cut $\chi^2(\Delta E) \leq 20$ and $\chi^2(\langle \beta^{-1} \rangle) \leq 20$ for $|Q| = 2/3e$ particles.

M \ β	0.30	0.35	0.40	0.45	0.50	0.55	0.60
0.938					90.0	99.2	99.1
1.875				97.0	99.1	99.6	99.9
5		86	99.6	99.5	99.5	99.7	99.3
10		99.2	99.5	99.5	99.3	99.3	99.6
15	78	99.2	99.7	99.7	99.4	99.7	99.4
20	86	99.7	99.5	99.7	99.5	99.8	99.6
24	87	99.4	99.7	99.8	99.5	99.2	99.8

Table 4

Integrated luminosity of the quark search

s (GeV^2)	2080	2830	3844
Luminosity (cm^{-2})	0.66×10^{35}	3.66×10^{35}	0.75×10^{32}

Table 5

Flux limits of quarks through telescopes (90% confidence level)

Telescope	Flux of quarks / Flux of normal particles		
	$s = 2830\ GeV^2$	$s = 2080\ GeV^2$	$s = 3844\ GeV^2$
A	$< 1.89 \times 10^{-9}$	$< 1.29 \times 10^{-8}$	$< 9.61 \times 10^{-6}$
W	$< 5.54 \times 10^{-9}$	$< 3.13 \times 10^{-8}$	$< 2.55 \times 10^{-5}$
α	$< 2.53 \times 10^{-9}$	$< 1.50 \times 10^{-8}$	$< 1.36 \times 10^{-6}$
β	$< 5.29 \times 10^{-9}$	$< 3.14 \times 10^{-8}$	$< 2.66 \times 10^{-5}$
δ	$< 1.33 \times 10^{-8}$	$< 6.55 \times 10^{-8}$	$< 5.74 \times 10^{-5}$
L	$< 4.29 \times 10^{-8}$	$< 1.65 \times 10^{-7}$	$< 2.32 \times 10^{-4}$
Total	$< 7.18 \times 10^{-10}$	$< 4.36 \times 10^{-9}$	$< 1.07 \times 10^{-6}$

Figure Captions

Fig. 1 : Measured cross-section limits from quark searches prior to 1972 (90% confidence level). Also shown are the predictions of three models, illustrating the range of theoretical expectations. The pair production cross-section by time-like photons was computed at $s = 2830\ GeV^2$. For $|Q| = 2/3e$ production, it is increased by a factor of four.

Fig. 2 : Design of a typical scintillation counter of a quark telescope. All counters were made from 20 mm thick Nuplex-3.

Fig. 3 : Layout of the quark detector in intersection region I4.

Fig. 4 : Schematic diagram of the trigger electronics for one telescope which provide the dE/dx and TOF triggers. The other five telescopes are similarly equipped. See text for explanation of the symbols.

Fig. 5 : Schematic diagram of the analog electronics for pulse-height registration. For each telescope only counter 1 is shown, the other eight channels are identical.

Fig. 6 : Comparison between measured and computed energy loss distribution for $\beta = 0.96$ pions in counter $\alpha 5$. The two spectra were normalized to the same height and position of the peak.

Fig. 7 : Measured and calculated veto level efficiency for $|Q| = 2/3e$ with the veto level set to $0.95\ \varepsilon_0$. The low β-measurements were obtained with protons and the high β-points with pions.

Fig. 8 : Momentum and mass range accepted with the dE/dx trigger. For $|Q| = 2/3e$ this range is restricted to the cross-hatched area above the line $\beta = 0.7$. For $|Q| = 1/3e$ the area above the line $\beta = 0.35$ is kinematically permitted.

Fig. 9 : Kinematically allowed momentum and mass range for the TOF trigger (hatched area). The range requirement $R > 24\ g\ cm^{-2}$ increases the low β cut-off for low masses. The indicated β limits, $\beta = 0.33$, 0.28, and 0.26 at masses 4, 7, and 10 GeV/c^2, respectively, apply to particles with charge $|Q| = 2/3e$.

Fig. 10 : Combined mass acceptance of the quark telescopes for isotropic production.

Fig. 11 : Combined mass acceptance of the quark telescope assuming $\langle p_T \rangle$ = = 0.4 GeV/c for the reaction products.

Fig. 12 : Measured and calculated distributions of $\ln \mathscr{L}$ for minimum ionizing $|Q|$ = 1e particles.

Fig. 13 : Measured and calculated distributions of $\ln \mathscr{L}$ for simulated $|Q|$ = 1/3e particles.

Fig. 14 : Standard deviation σ_i for the measured β_i^{-1} distributions as a function of the most probable energy loss ε_p.

Fig. 15 : $\ln \mathscr{L}$ distributions of all data with $\varepsilon_p \leq 0.42\ \varepsilon_0$.

Fig. 16 : $\ln \mathscr{L}$ distribution of all data with $\varepsilon_p > 0.42\ \varepsilon_0$.

Fig. 17 : $\ln \mathscr{L}$ distribution for all data with $\varepsilon_p \leq 0.42\ \varepsilon_0$, with and without a good timing cut.

Fig. 18 : $\chi^2(\langle \beta^{-1} \rangle)$ distributions for two data samples with $0.3\ \varepsilon_0 \leq \varepsilon_p \leq 0.42\ \varepsilon_0$ (right scale) and $\varepsilon_p < 0.15\ \varepsilon_0$ (left scale).

Fig. 19 : Average energy loss and width of the distributions for slow protons as a function of depth into the telescope; the bars on the measured and calculated points indicate the 2σ width of the distributions.

Fig. 20 : The $\chi^2(\Delta E)$ distribution for protons as measured and as calculated for a Monte Carlo sample of protons with the same velocity spectrum as our data.

Fig. 21 : $|Q/e|$ distribution of all TOF data after χ^2 cuts, together with a simulated distribution for a M = 10 GeV/c^2, $|Q|$ = 2/3e quark.

Fig. 22 : Cross-section limits at s = 2830 GeV^2 for $|Q|$ = 1/3e for the model assuming $\langle p_T \rangle$ = 0.4 GeV/c. Shown are our previously published results and the final limits of this experiment. The curves represent the 90% confidence limits.

Fig. 23 : Cross-section limits at s = 2830 GeV^2 for $|Q|$ = 2/3e for the model assuming $\langle p_T \rangle$ = 0.4 GeV/c. Shown are our previously published results and the final limits of this experiment. The curves represent the 90% confidence limits.

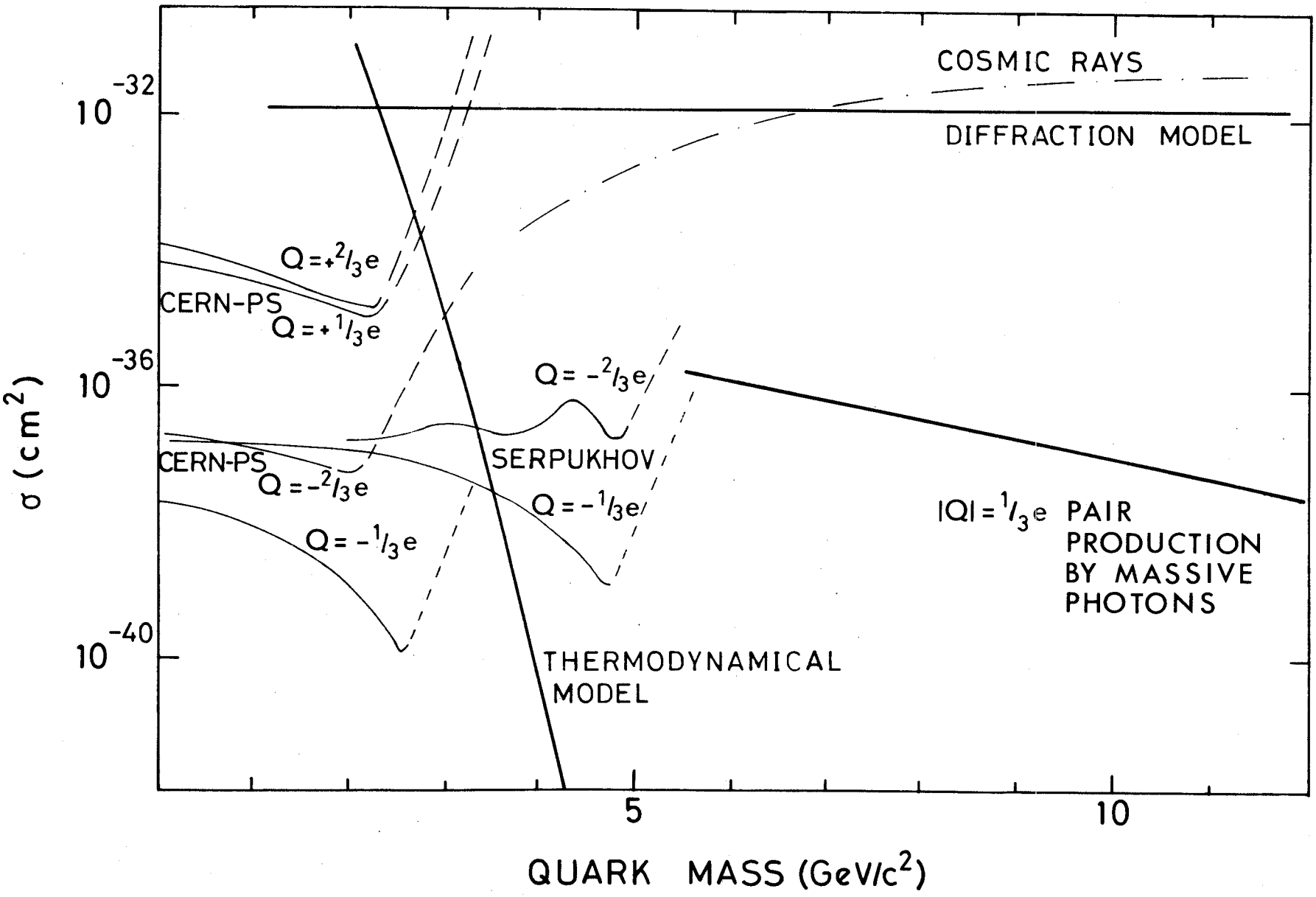
COSMIC RAYS
DIFFRACTION MODEL
$Q = +^2/_3 e$
CERN-PS
$Q = +^1/_3 e$
$Q = -^2/_3 e$
SERPUKHOV
CERN-PS
$Q = -^2/_3 e$
$Q = -^1/_3 e$
$Q = -^1/_3 e$
$|Q| = ^1/_3 e$ PAIR PRODUCTION BY MASSIVE PHOTONS
THERMODYNAMICAL MODEL
10^{-32}
10^{-36}
10^{-40}
$\sigma\ (cm^2)$
5
10
QUARK MASS (GeV/c^2)

Fig. 1

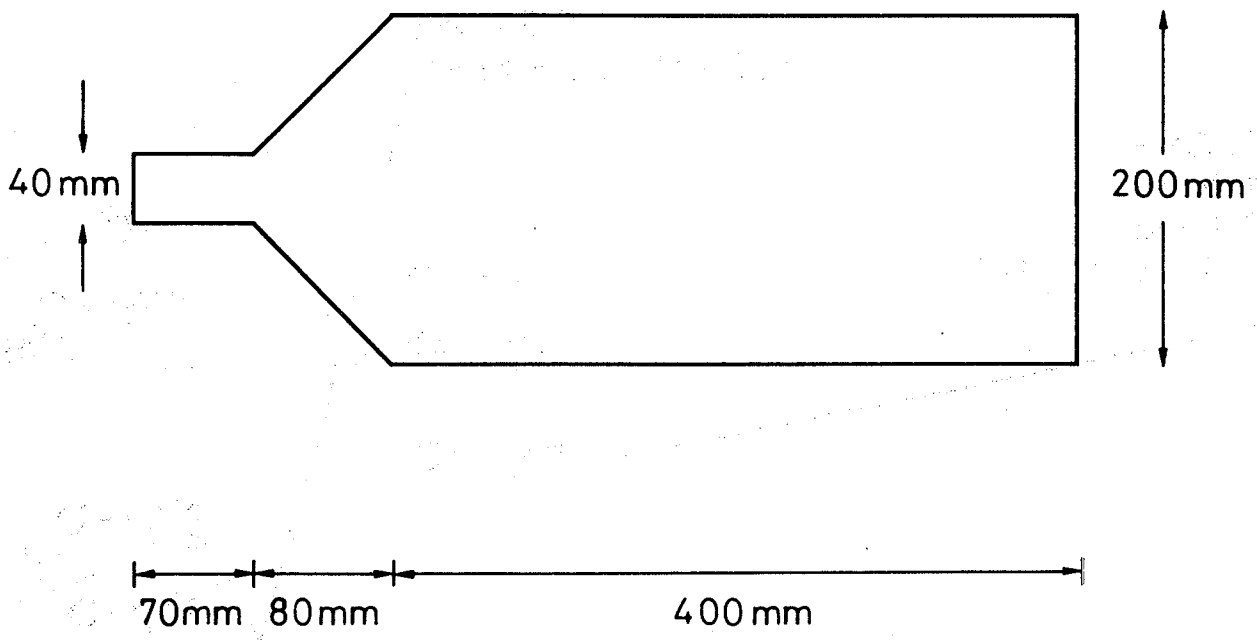

Fig. 2

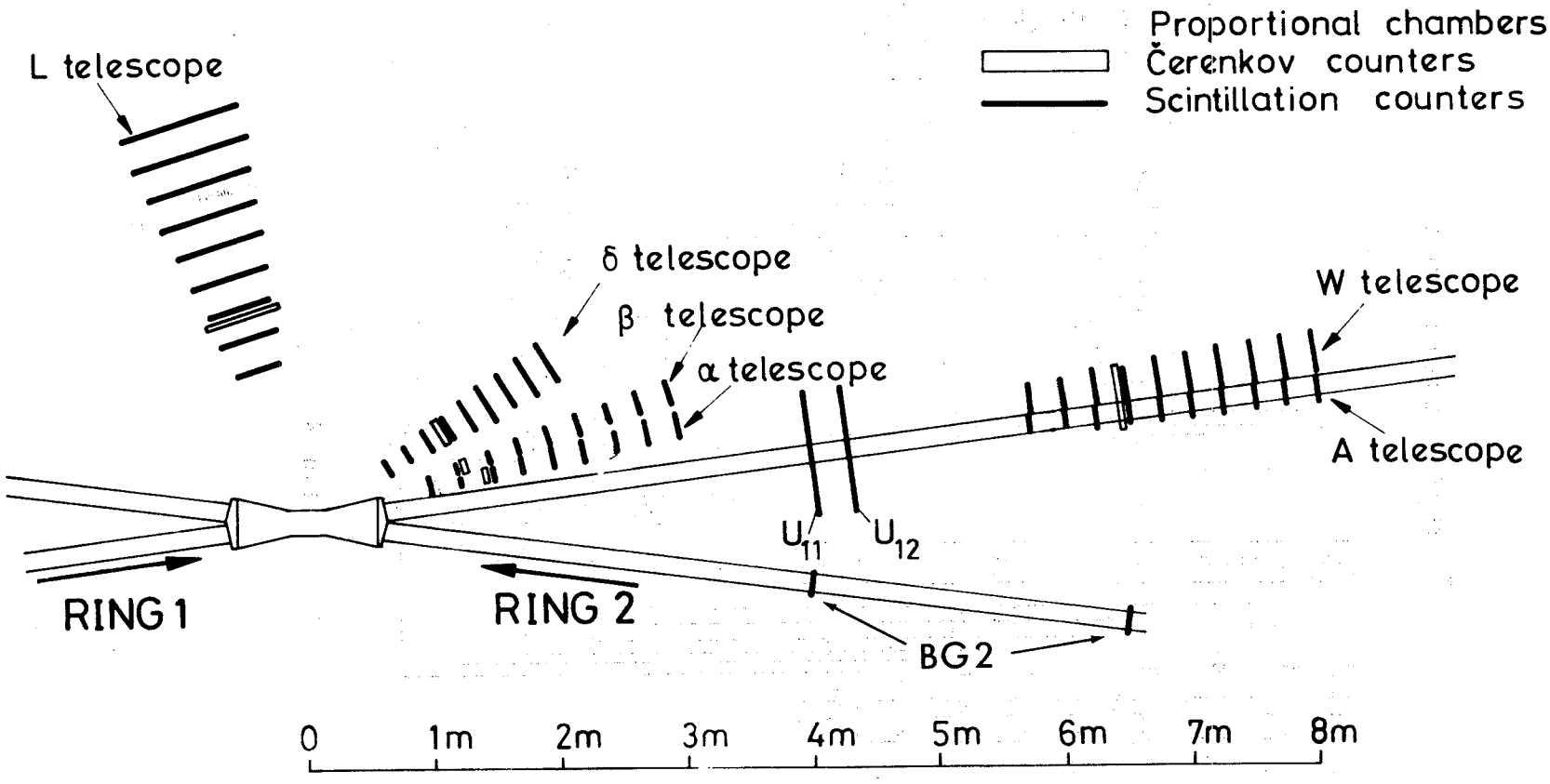
Proportional chambers
Čerenkov counters
Scintillation counters
L telescope
δ telescope
β telescope
α telescope
W telescope
A telescope
U_{11}
U_{12}
RING 1
RING 2
BG 2
0
1m
2m
3m
4m
5m
6m
7m
8m

Fig. 3

Trigger Electronics

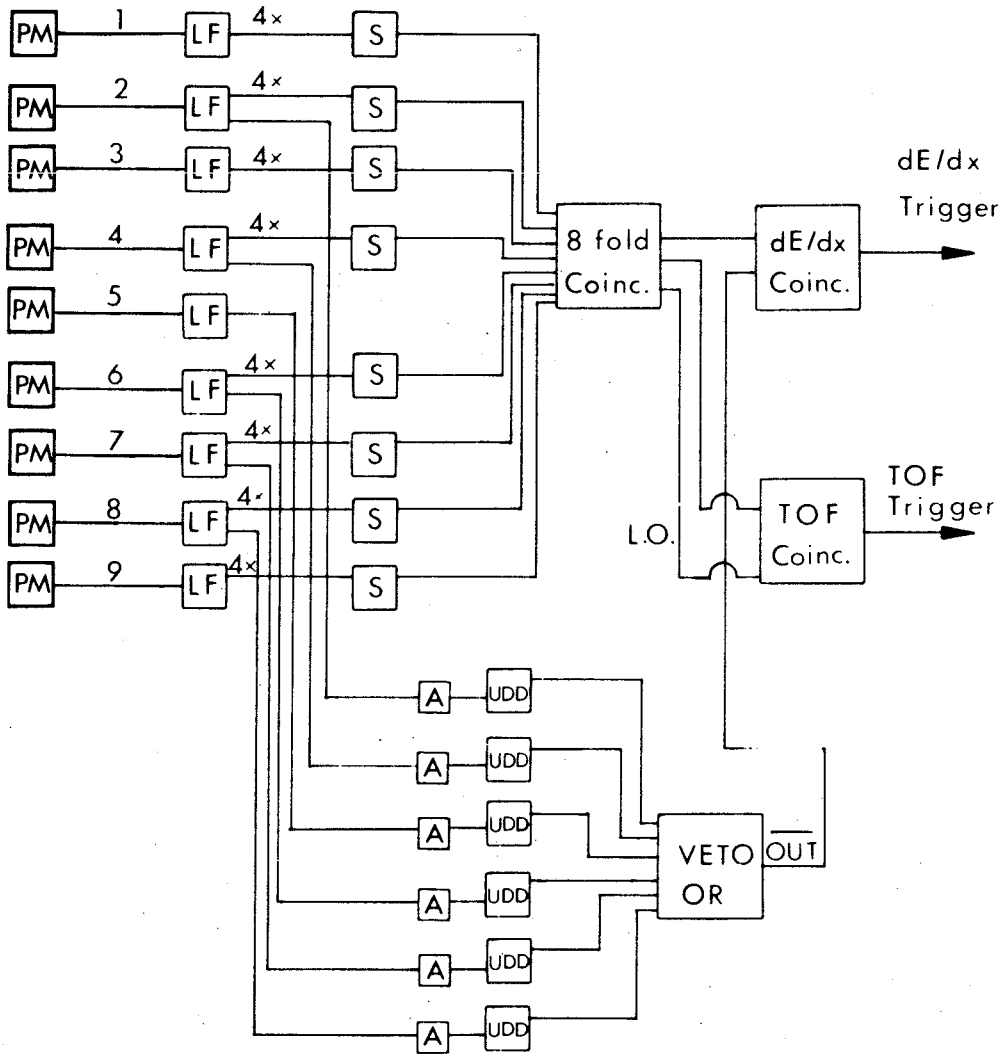

Fig. 4

Analog Electronics

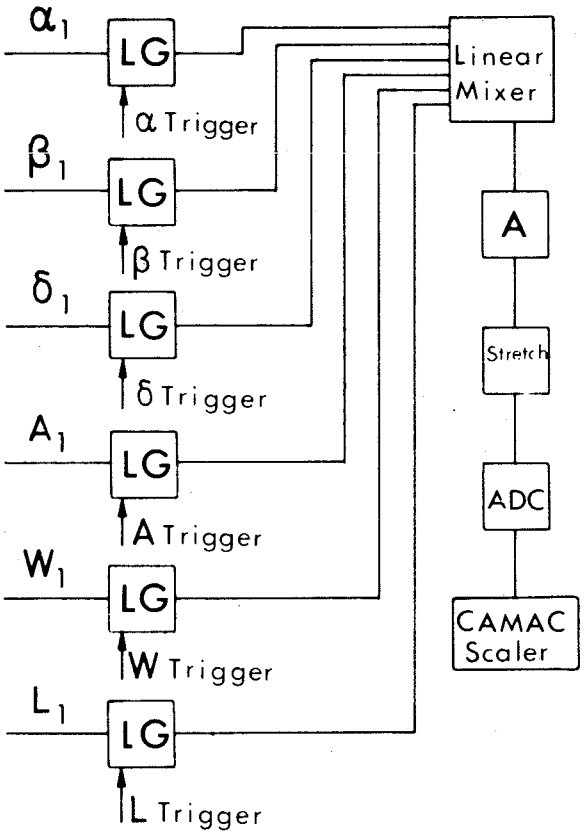

Fig. 5

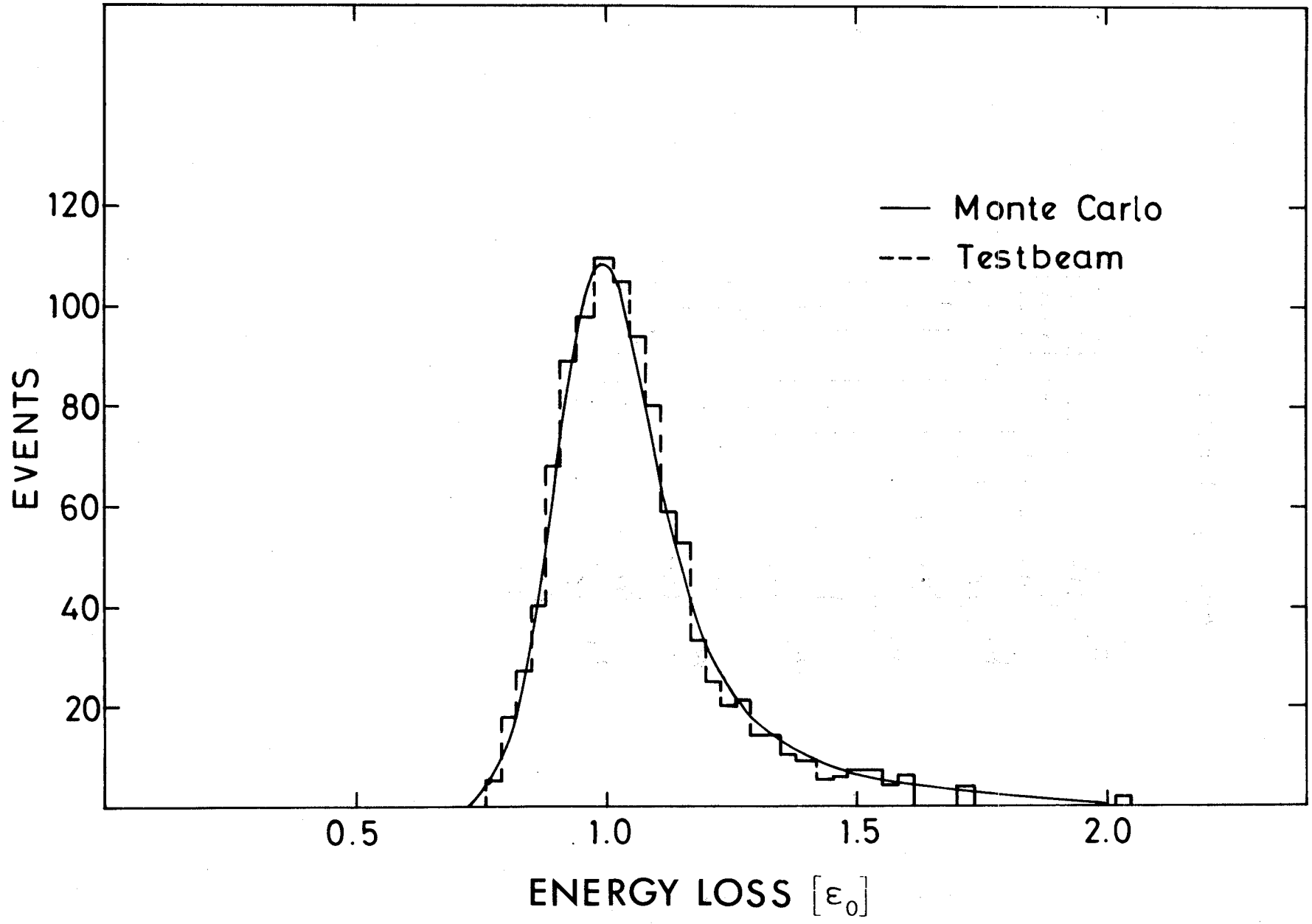
Monte Carlo
Testbeam
EVENTS
120
100
80
60
40
20
0.5
1.0
1.5
2.0
ENERGY LOSS [ε_0]

Fig. 6

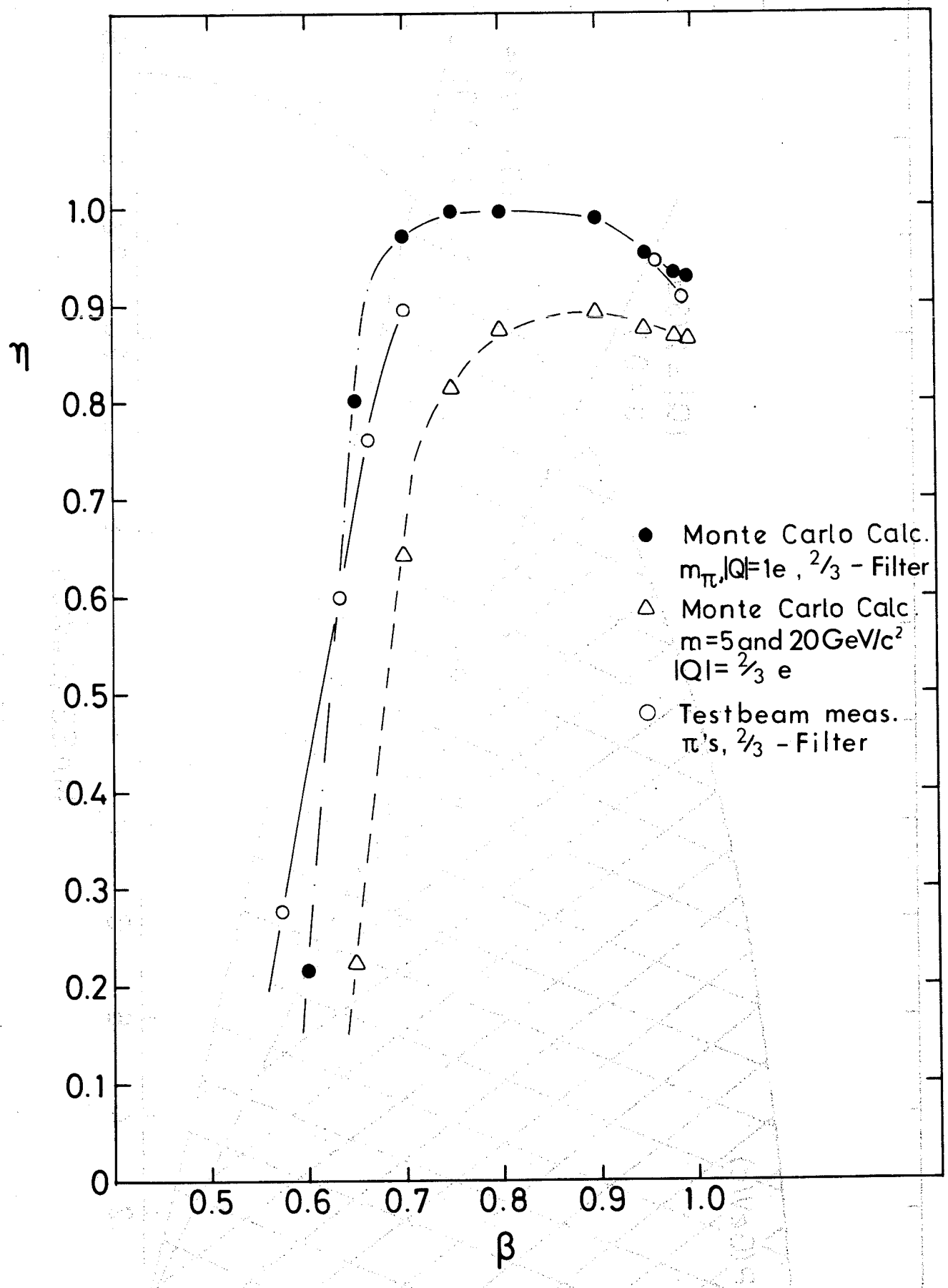
η
β
1.0
0.9
0.8
0.7
0.6
0.5
0.4
0.3
0.2
0.1
0
0.5
0.6
0.7
0.8
0.9
1.0
Monte Carlo Calc.
m_π, |Q|=1e , 2/3 - Filter
Monte Carlo Calc.
m=5 and 20 GeV/c²
|Q|= 2/3 e
Testbeam meas.
π's, 2/3 - Filter

Fig. 7

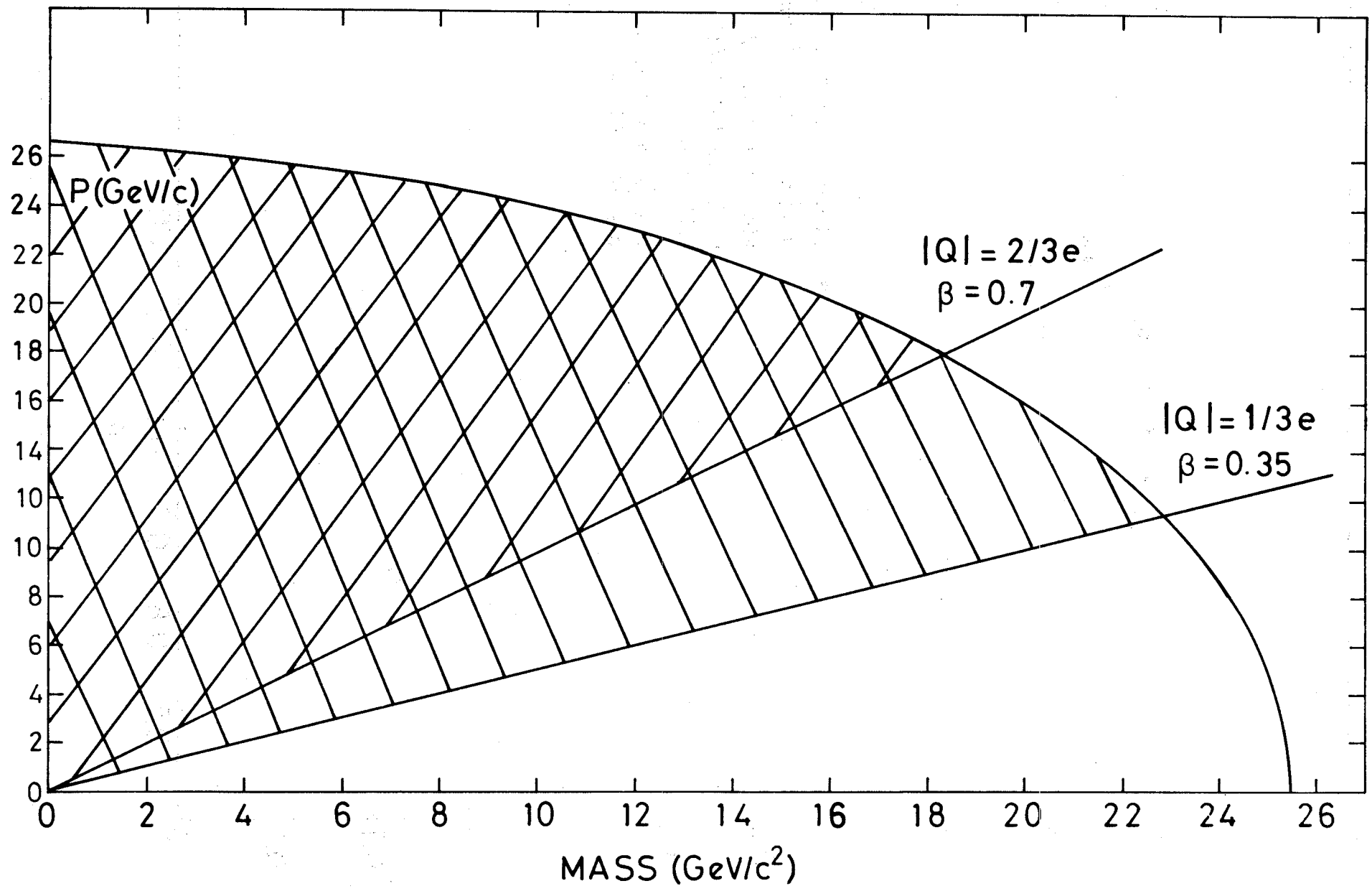
P(GeV/c)
|Q| = 2/3e
β = 0.7
|Q| = 1/3e
β = 0.35
0
2
4
6
8
10
12
14
16
18
20
22
24
26
MASS (GeV/c²)

Fig. 8

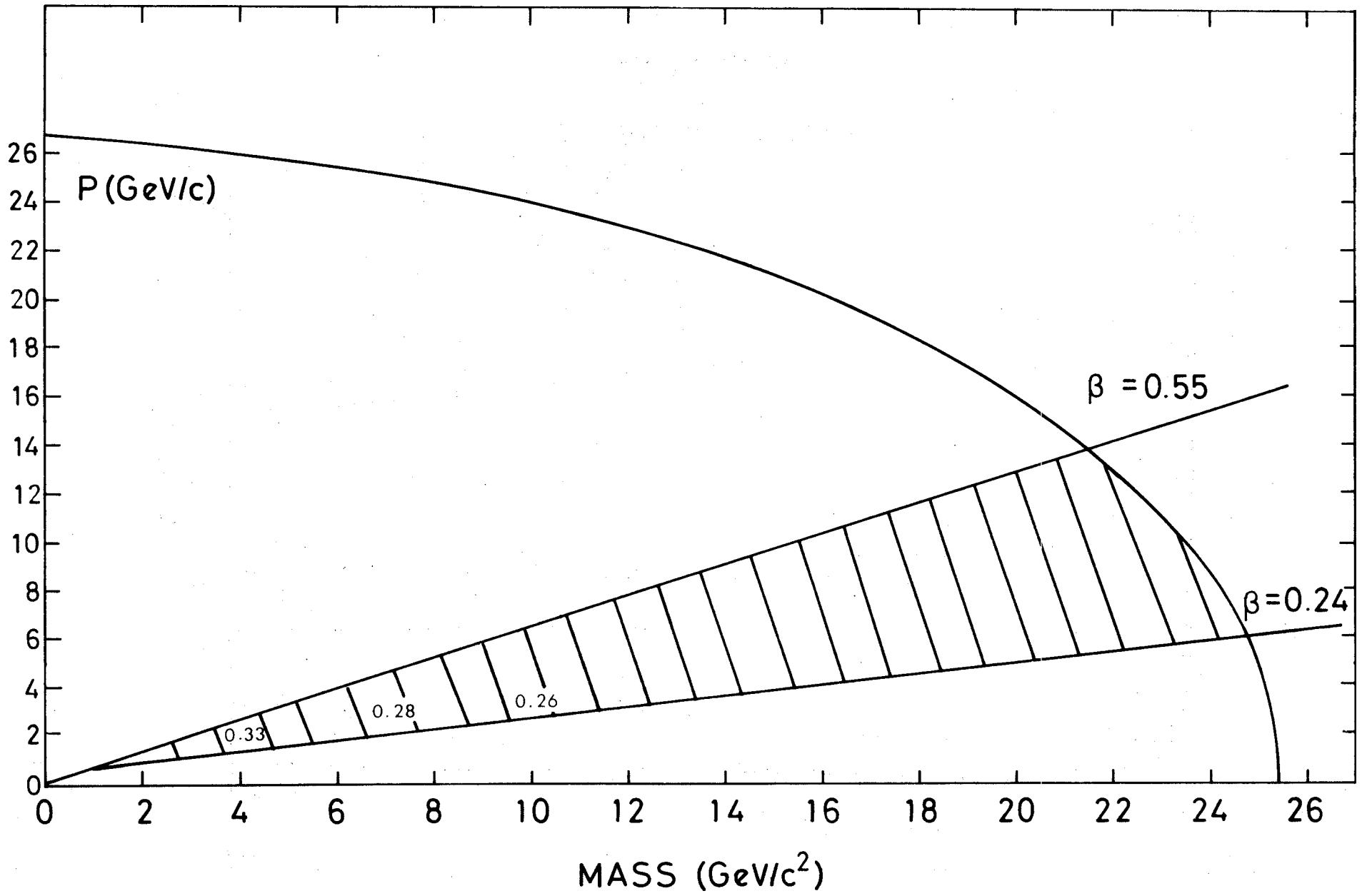
P (GeV/c)
β = 0.55
β = 0.24
0.33
0.28
0.26
MASS (GeV/c²)
0
2
4
6
8
10
12
14
16
18
20
22
24
26

Fig. 9

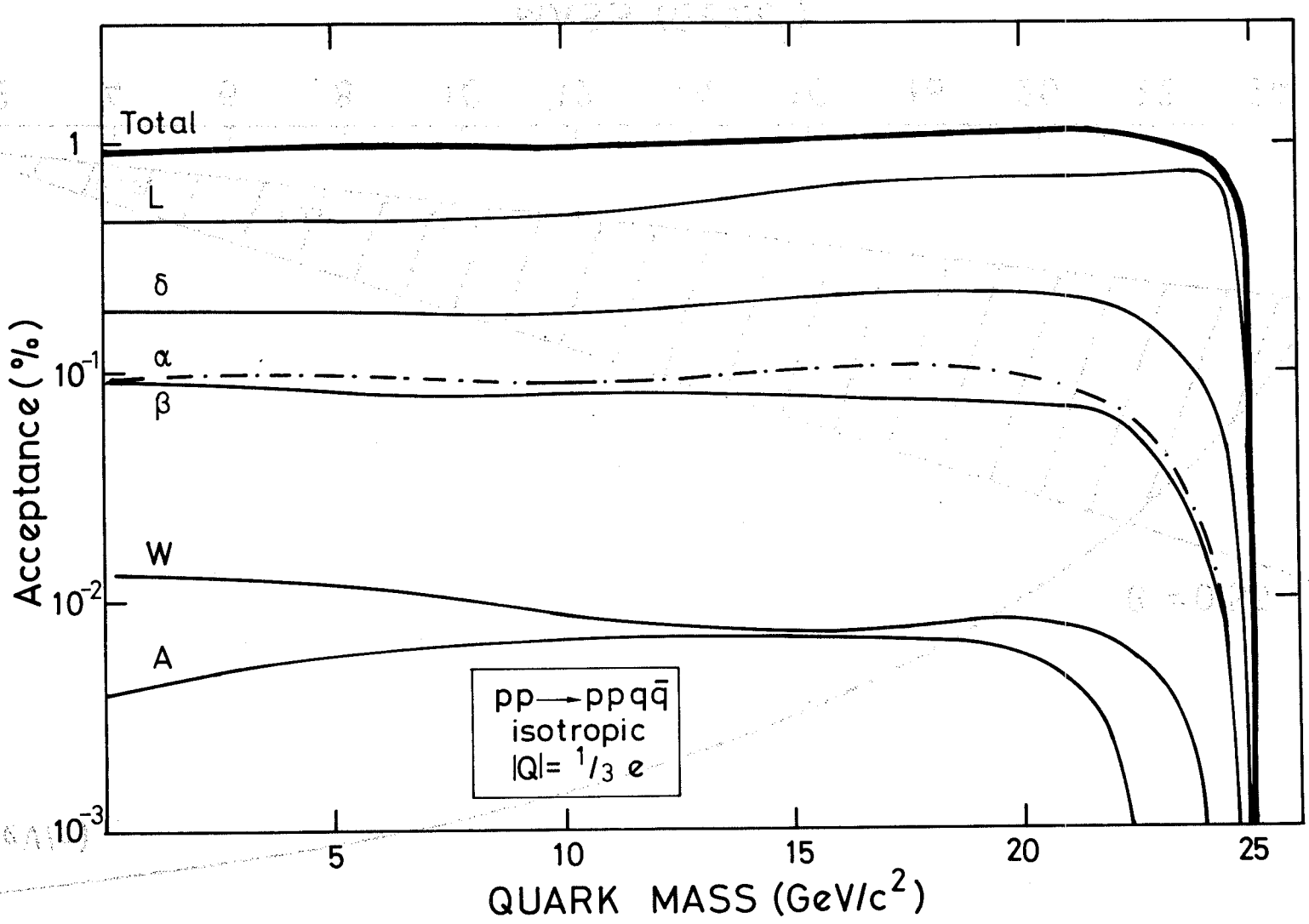
Total
L
δ
α
β
W
A
1
10^{-1}
10^{-2}
10^{-3}
Acceptance (%)
5
10
15
20
25
QUARK MASS (GeV/c^2)
pp⟶ppqq̄
isotropic
|Q|= 1/3 e

Fig. 10

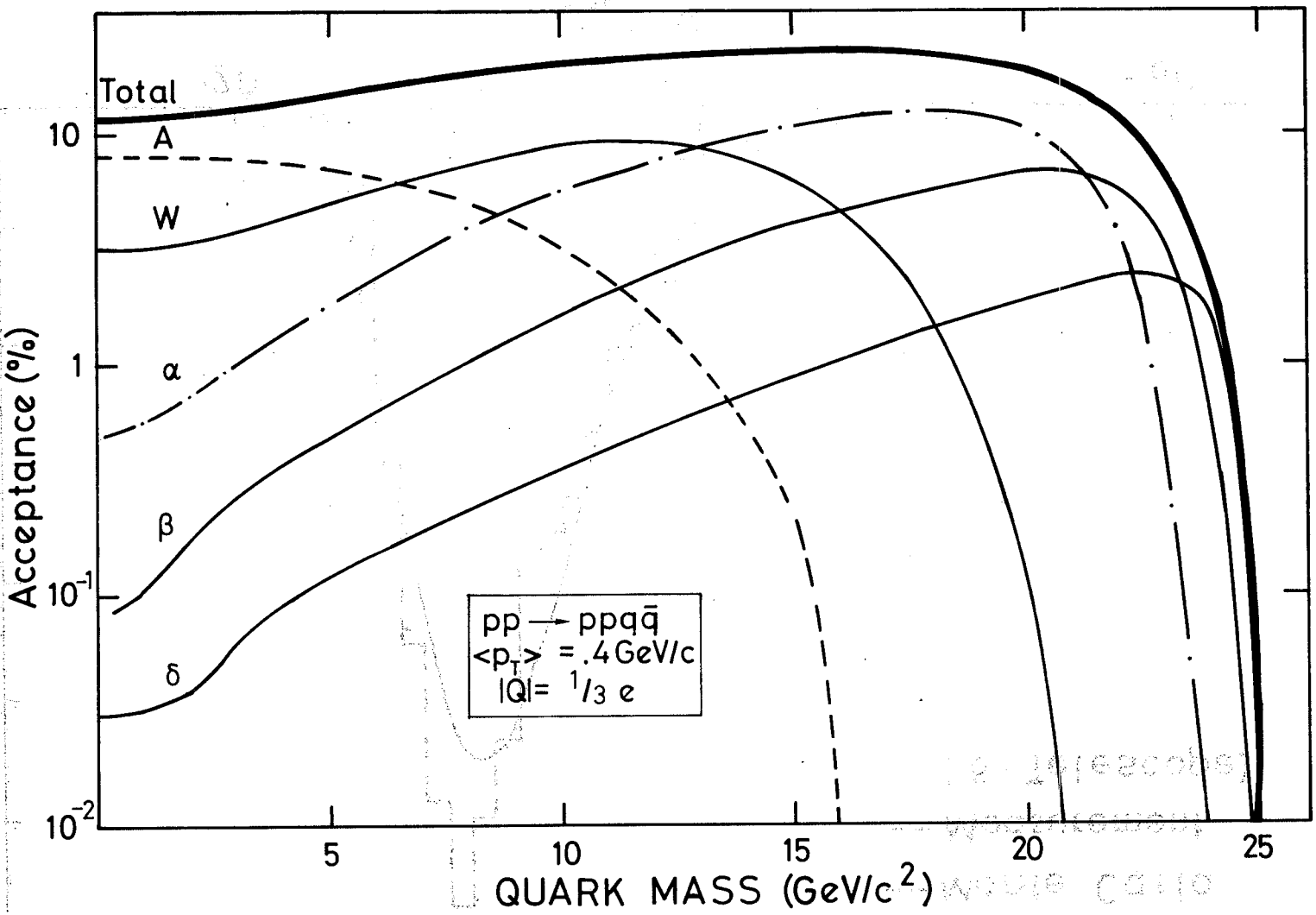
Total
A
W
α
β
δ
10
1
10^{-1}
10^{-2}
Acceptance (%)
$pp \rightarrow ppq\bar{q}$
$\langle p_T \rangle$ = .4 GeV/c
|Q| = 1/3 e
5
10
15
20
25
QUARK MASS (GeV/c^2)

Fig. 11

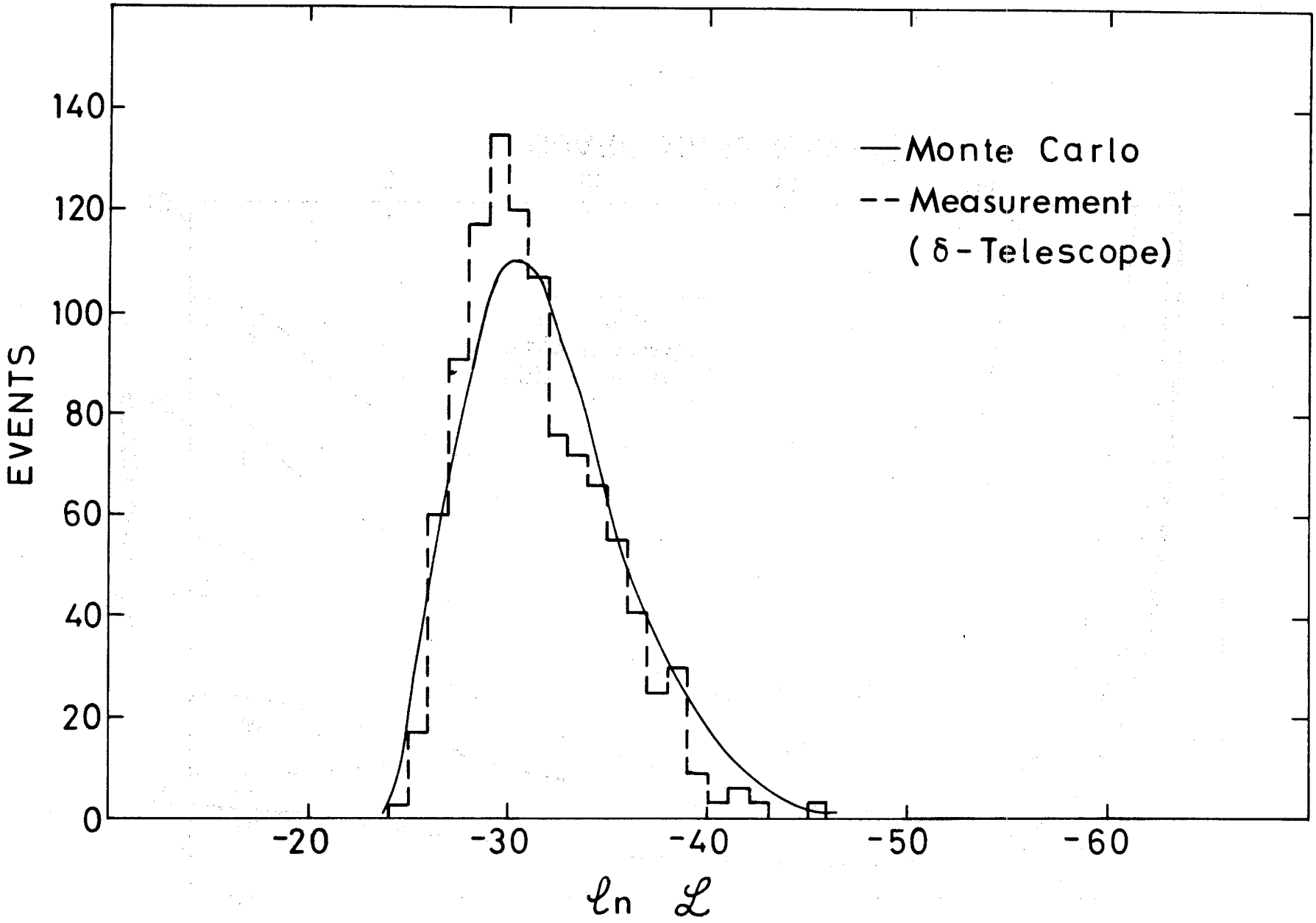
EVENTS
140
120
100
80
60
40
20
0
-20
-30
-40
-50
-60
ℓn ℒ
—Monte Carlo
-- Measurement
(δ - Telescope)

Fig. 12

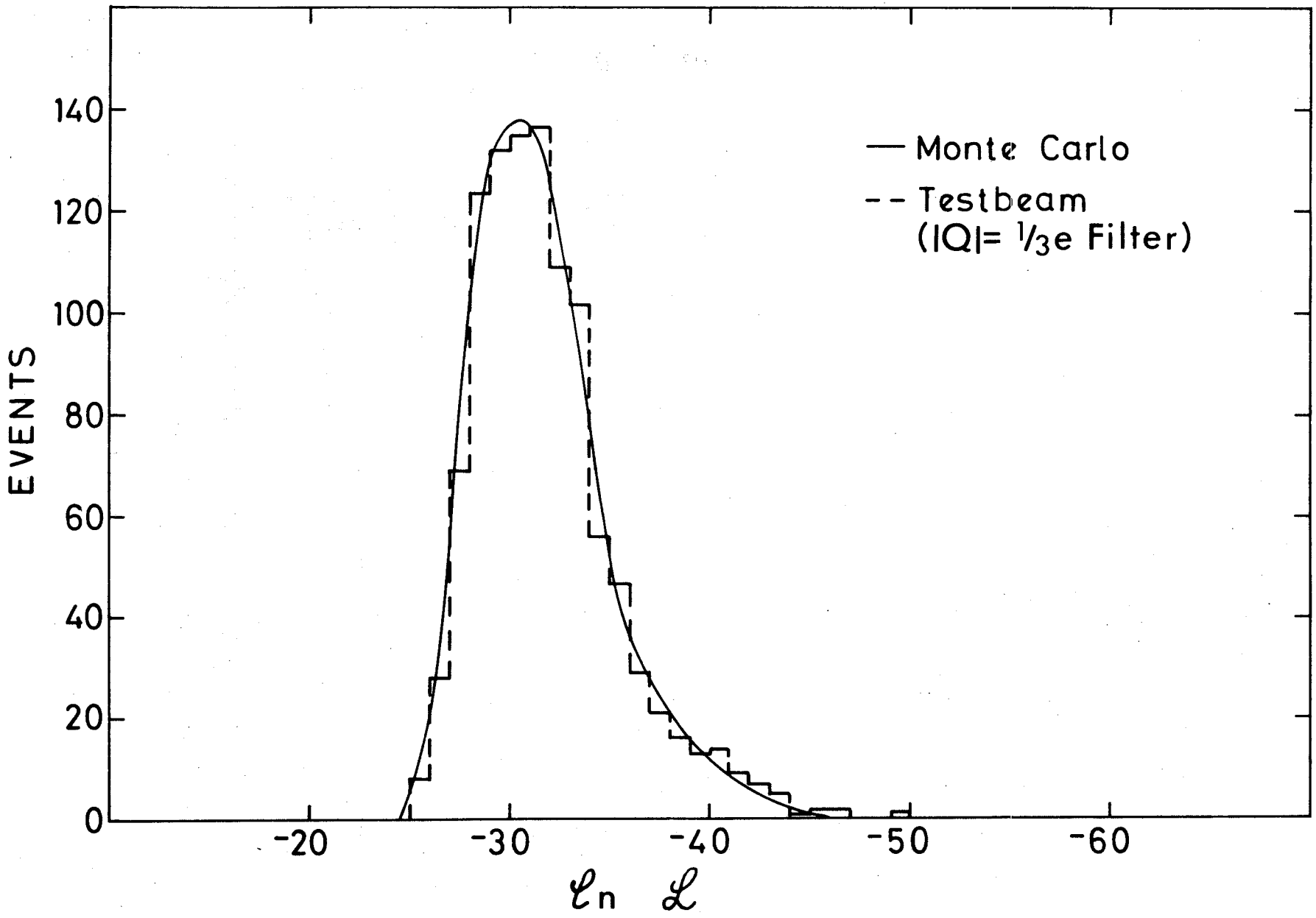
EVENTS
140
120
100
80
60
40
20
0
-20
-30
-40
-50
-60
ℓn ℒ
— Monte Carlo
-- Testbeam
(|Q|= 1/3e Filter)

Fig. 13

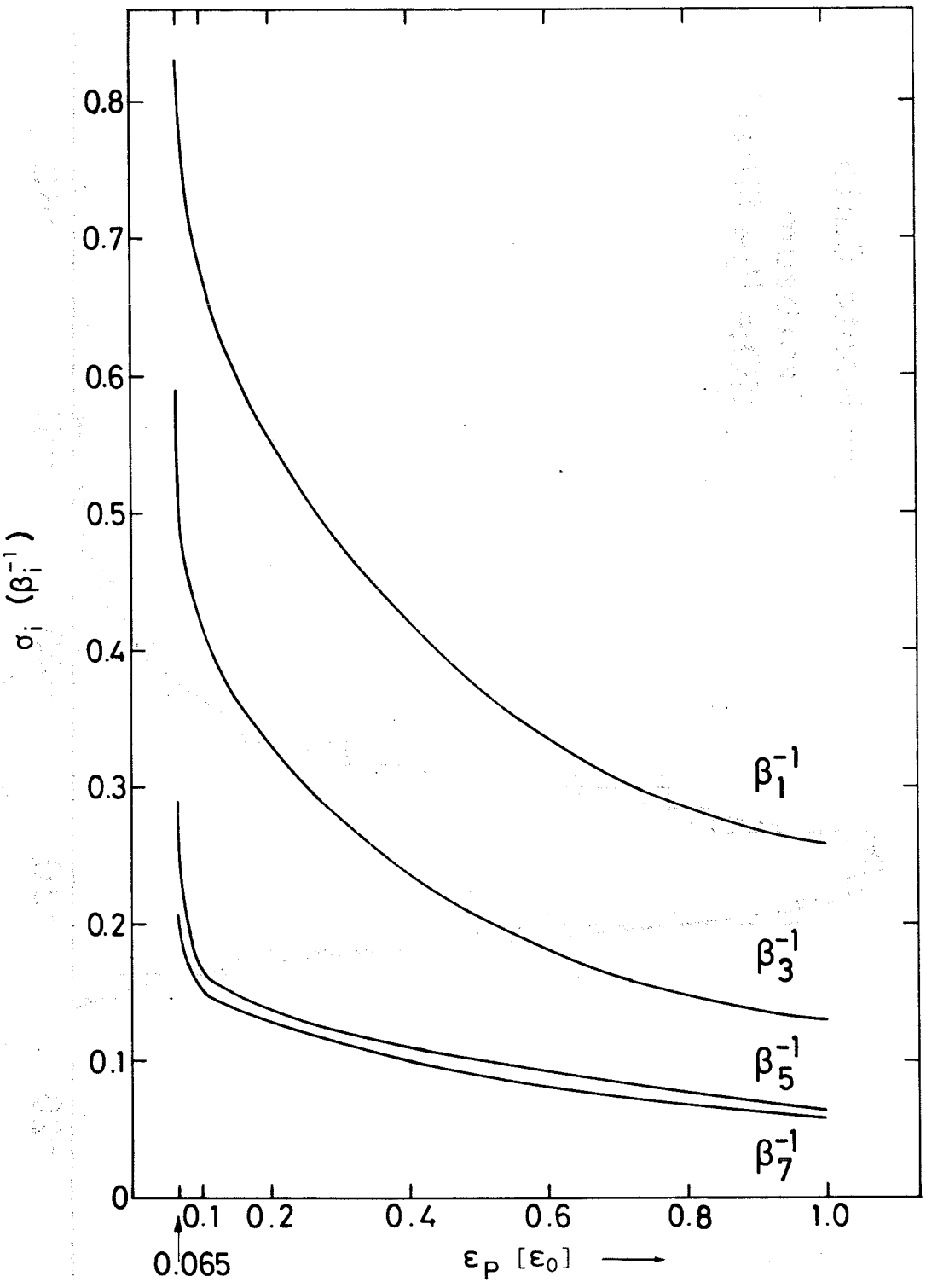
0.8
0.7
0.6
0.5
0.4
0.3
0.2
0.1
0
σ_i (β_i^{-1})
β_1^{-1}
β_3^{-1}
β_5^{-1}
β_7^{-1}
0.1
0.2
0.4
0.6
0.8
1.0
0.065
ε_P [ε_0] ⟶

Fig. 14

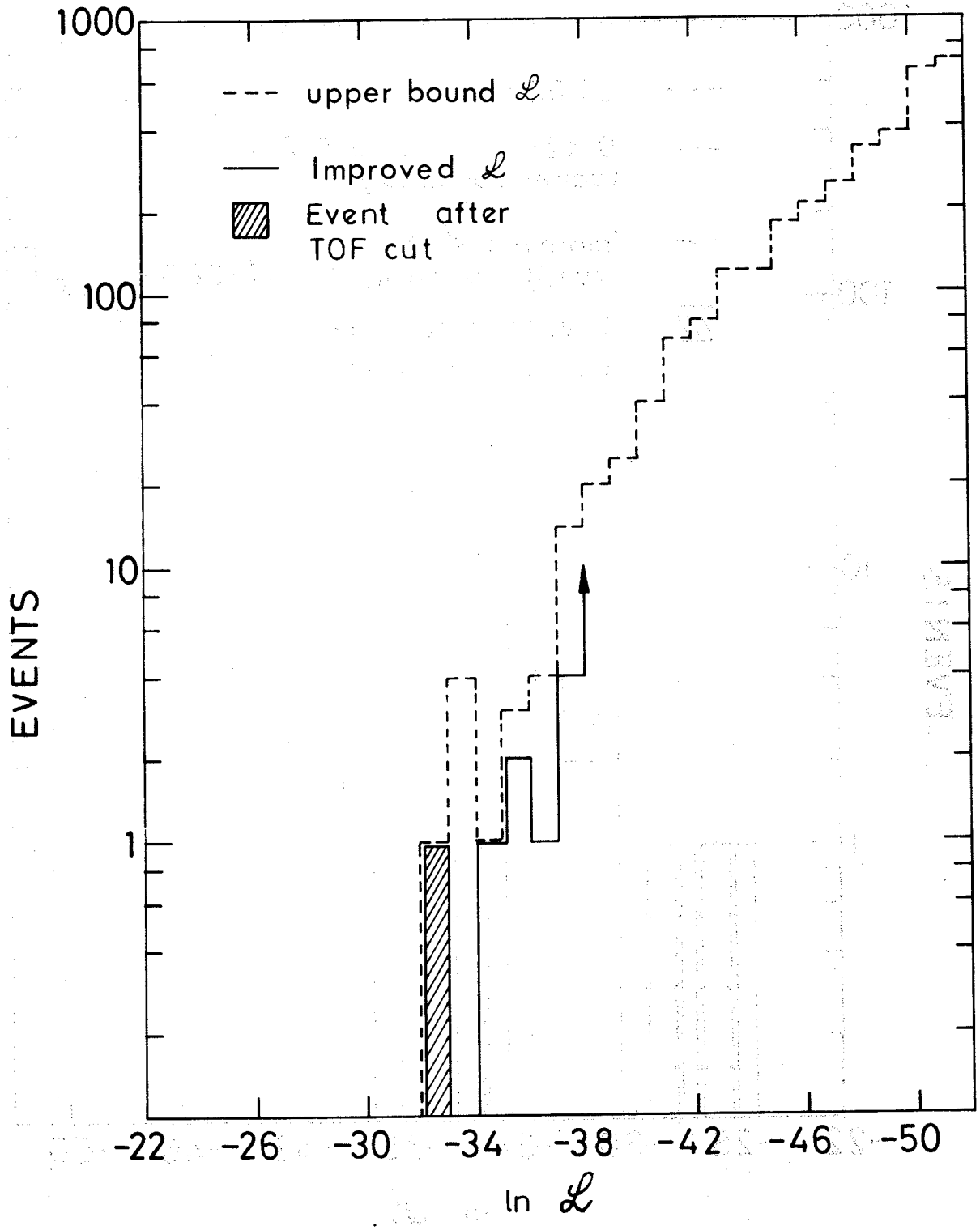
1000
100
10
1
EVENTS
upper bound ℒ
Improved ℒ
Event after
TOF cut
-22
-26
-30
-34
-38
-42
-46
-50
ln ℒ

Fig. 15

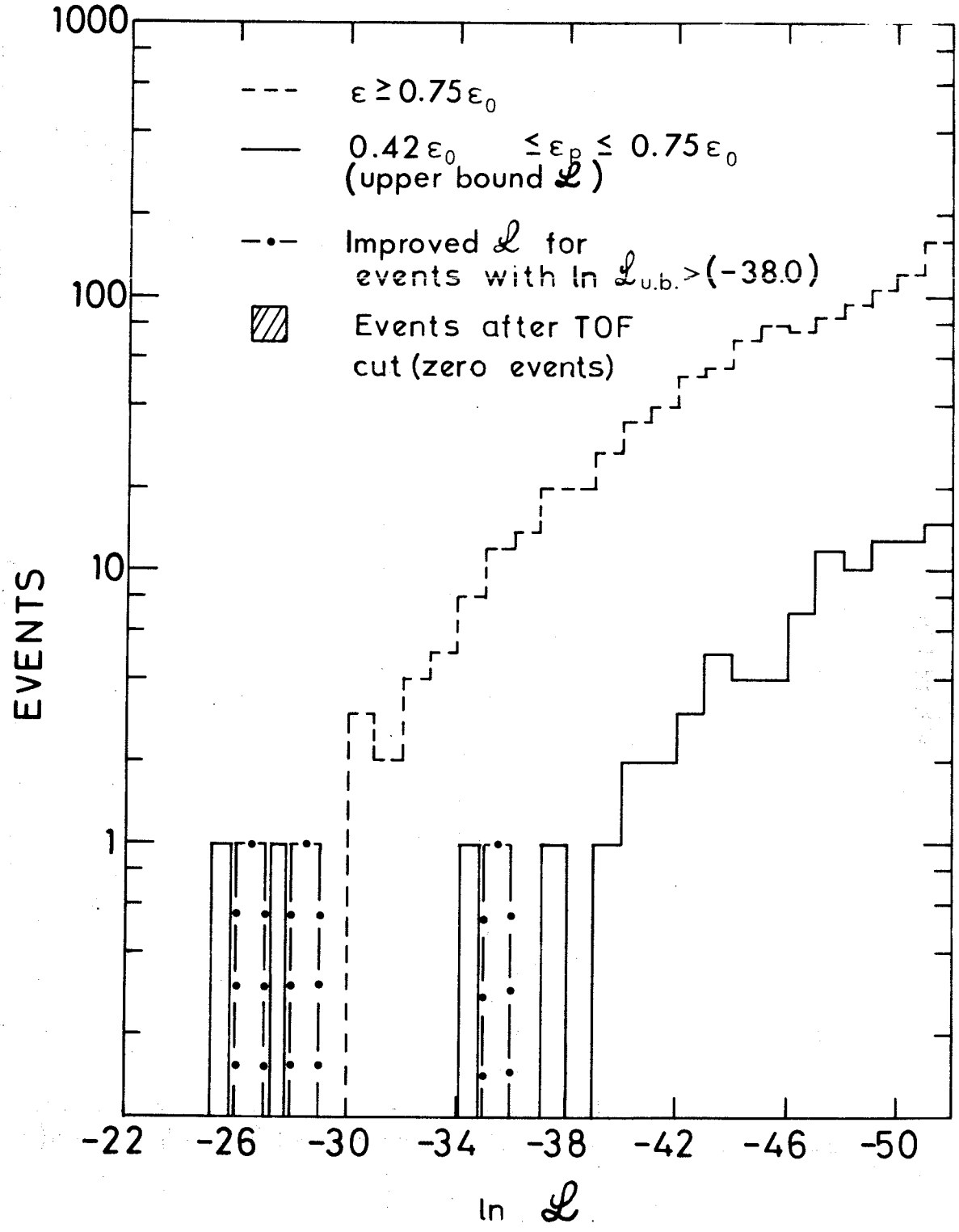
1000
100
10
1
EVENTS
$\varepsilon \geq 0.75\varepsilon_0$
$0.42\varepsilon_0 \leq \varepsilon_p \leq 0.75\varepsilon_0$
(upper bound $\mathscr{L}$)
Improved $\mathscr{L}$ for
events with ln $\mathscr{L}_{u.b.} > (-38.0)$
Events after TOF
cut (zero events)
-22
-26
-30
-34
-38
-42
-46
-50
ln $\mathscr{L}$

Fig. 16

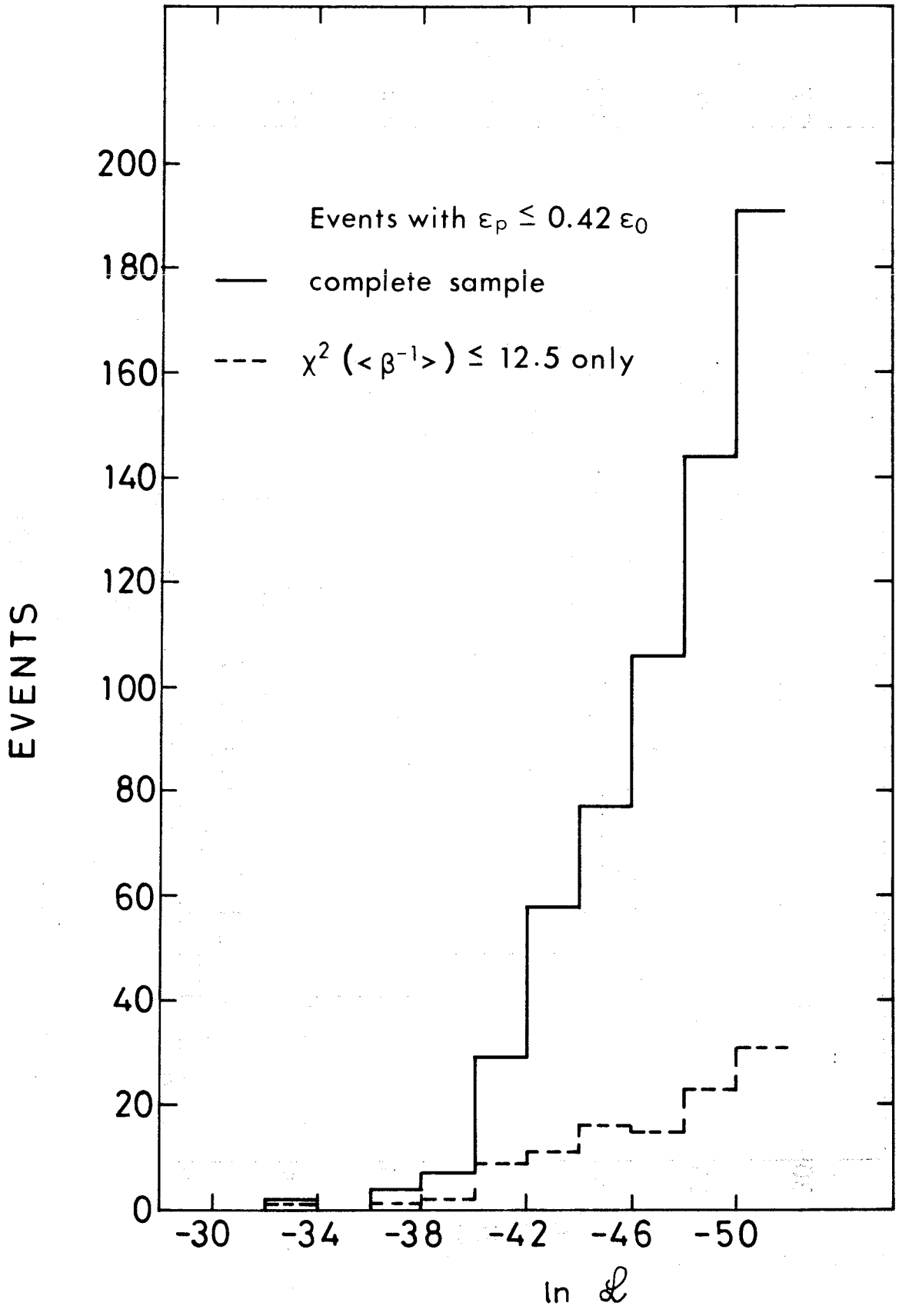
Events with $\varepsilon_p \leq 0.42\,\varepsilon_0$
complete sample
$\chi^2\,(<\beta^{-1}>) \leq 12.5$ only
EVENTS
200
180
160
140
120
100
80
60
40
20
0
-30
-34
-38
-42
-46
-50
ln $\mathscr{L}$

Fig. 17

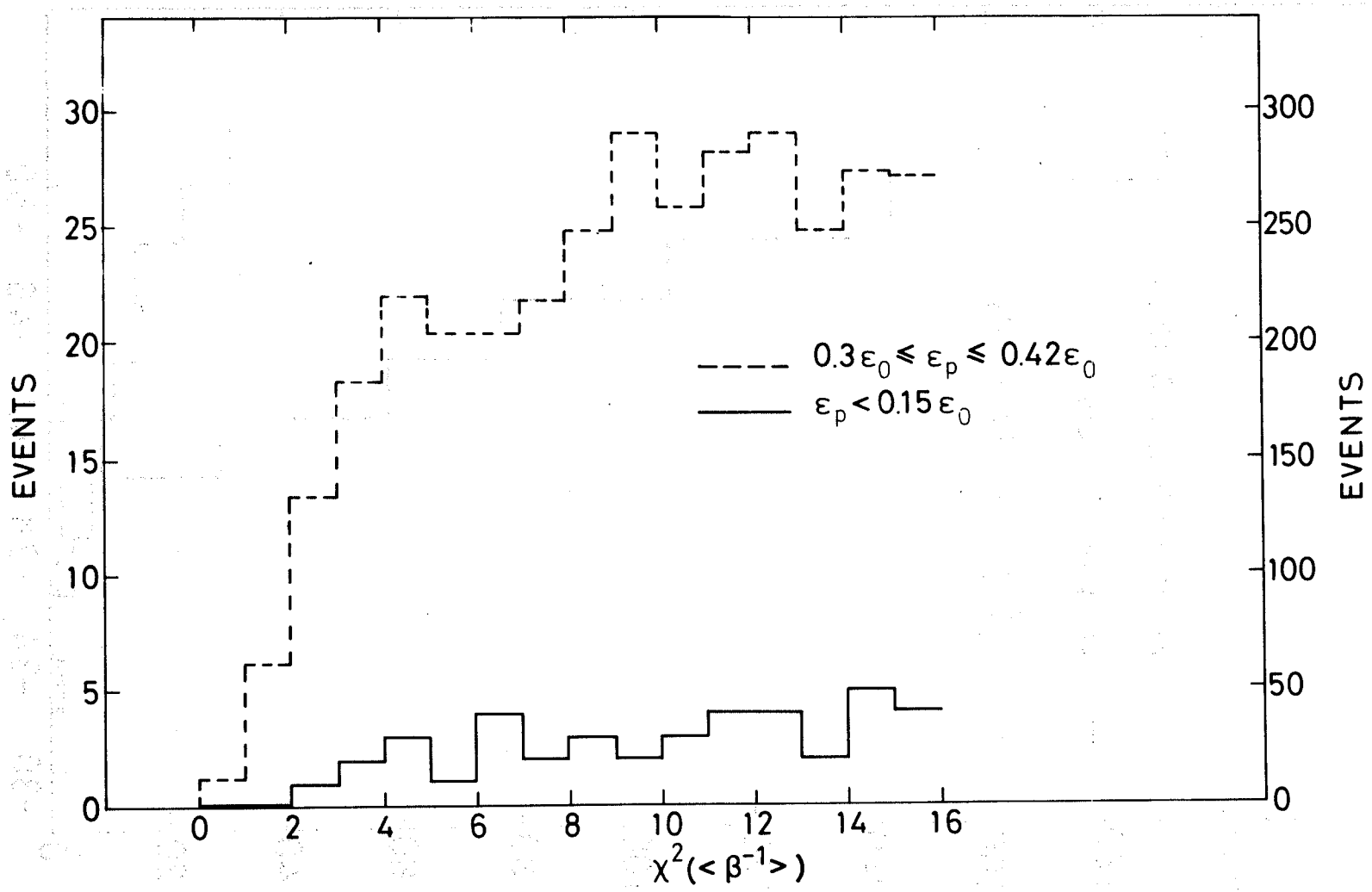
EVENTS
EVENTS
30
25
20
15
10
5
0
300
250
200
150
100
50
0
0
2
4
6
8
10
12
14
16
$\chi^2(<\beta^{-1}>)$
$0.3\varepsilon_0 \leq \varepsilon_p \leq 0.42\varepsilon_0$
$\varepsilon_p < 0.15\varepsilon_0$

Fig. 18

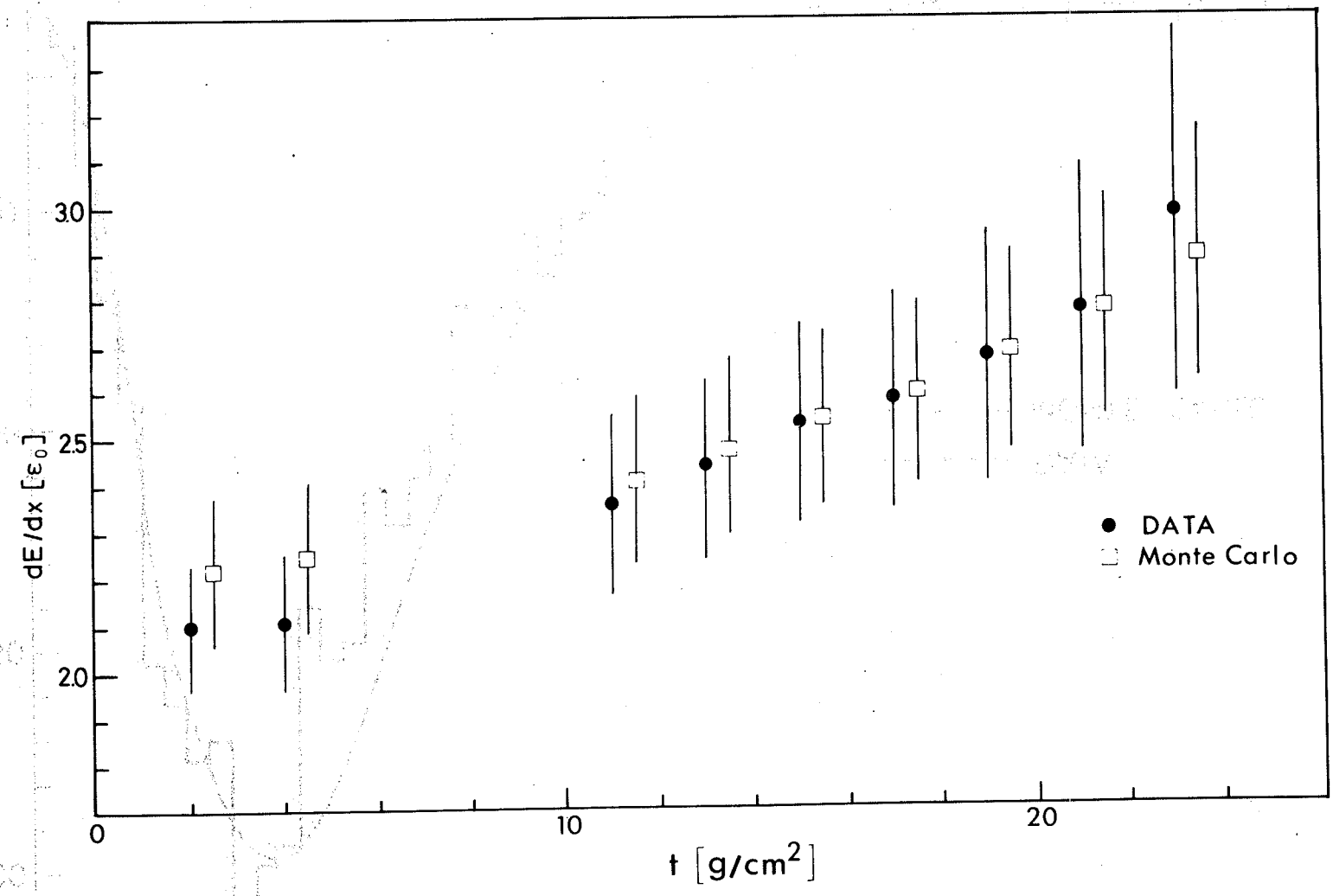

Fig. 19

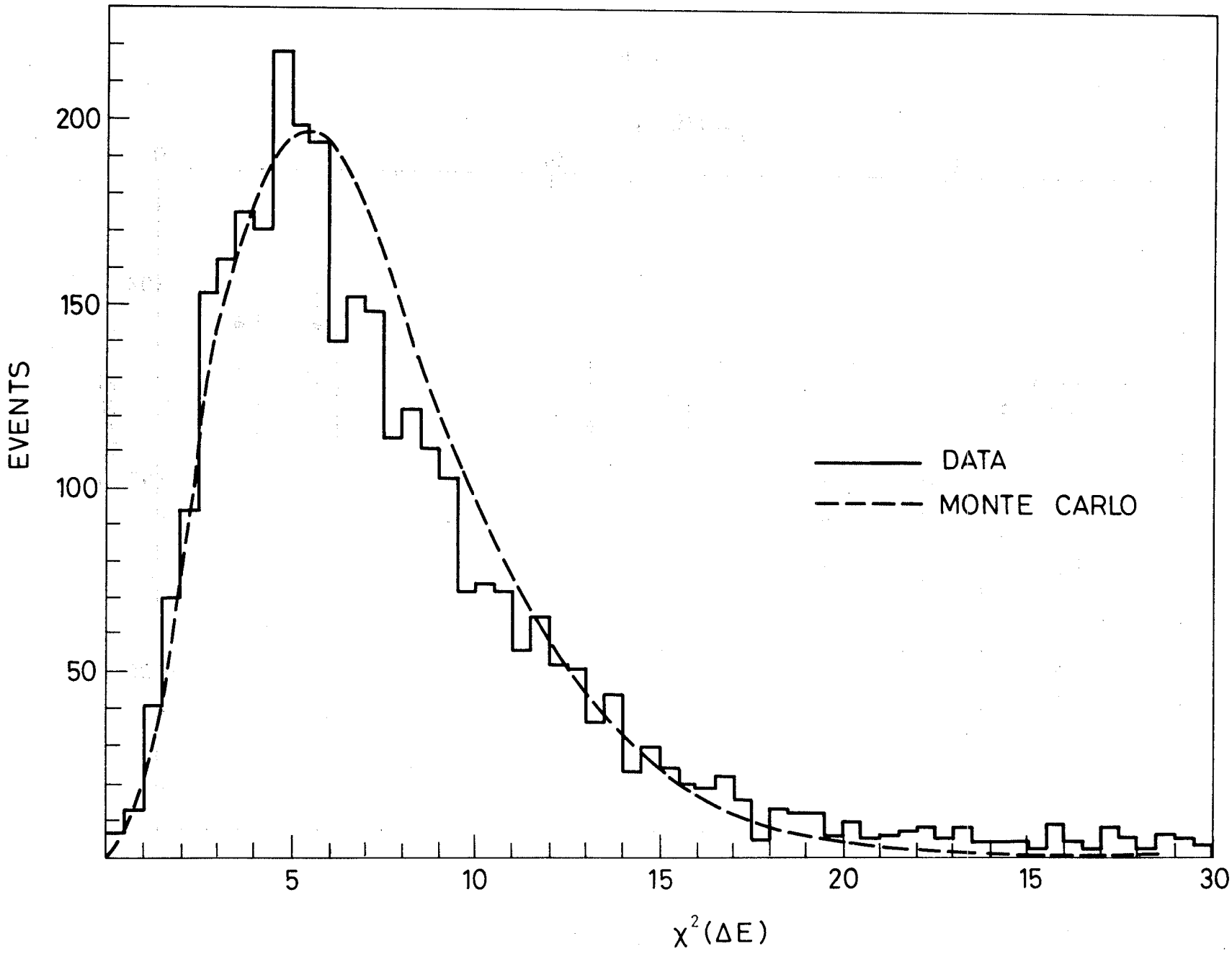
EVENTS
200
150
100
50
5
10
15
20
15
30
$\chi^2(\Delta E)$
DATA
MONTE CARLO

Fig. 20

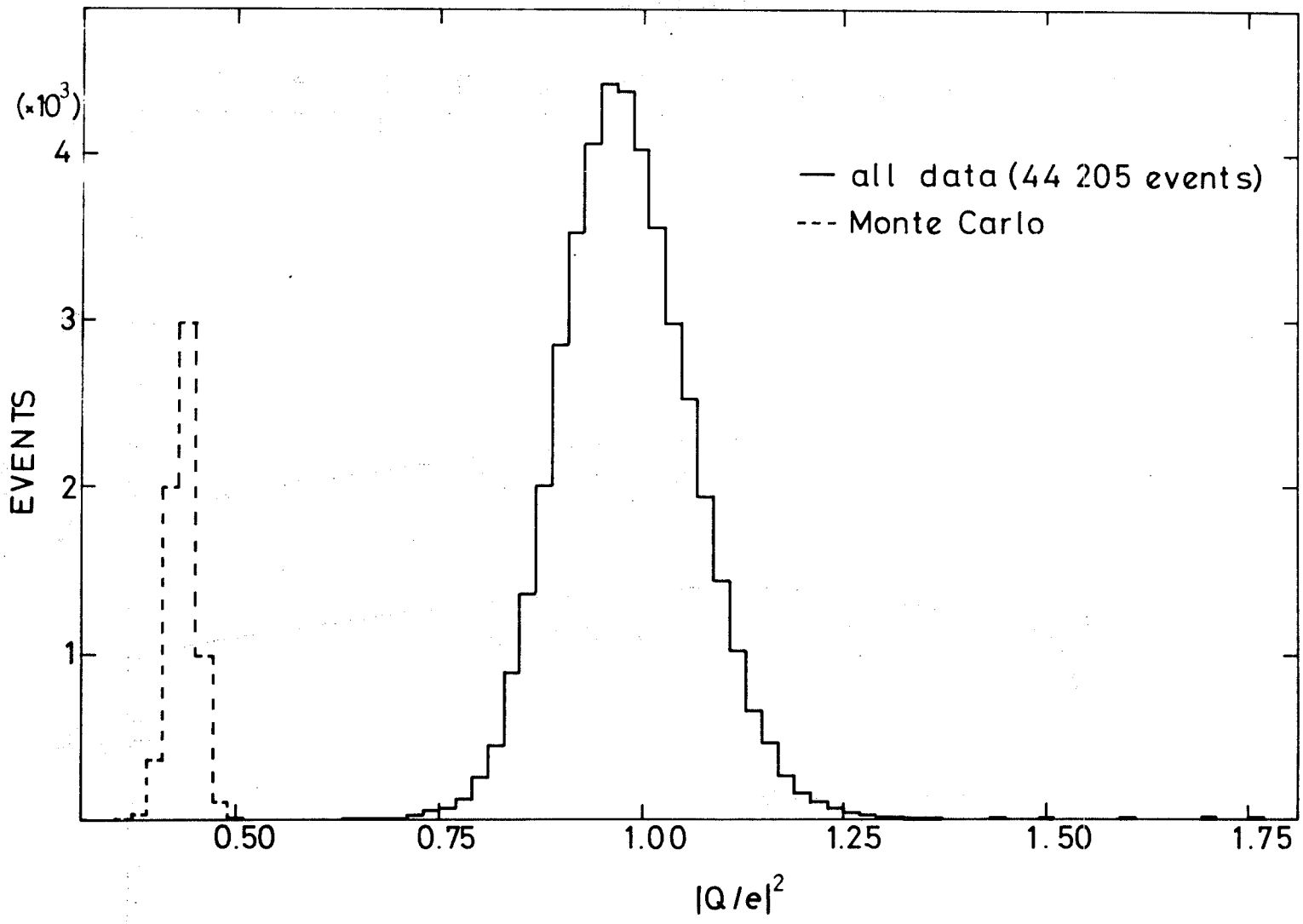
(×10³)
4
3
2
1
EVENTS
— all data (44 205 events)
--- Monte Carlo
0.50
0.75
1.00
1.25
1.50
1.75
|Q/e|²

Fig. 21

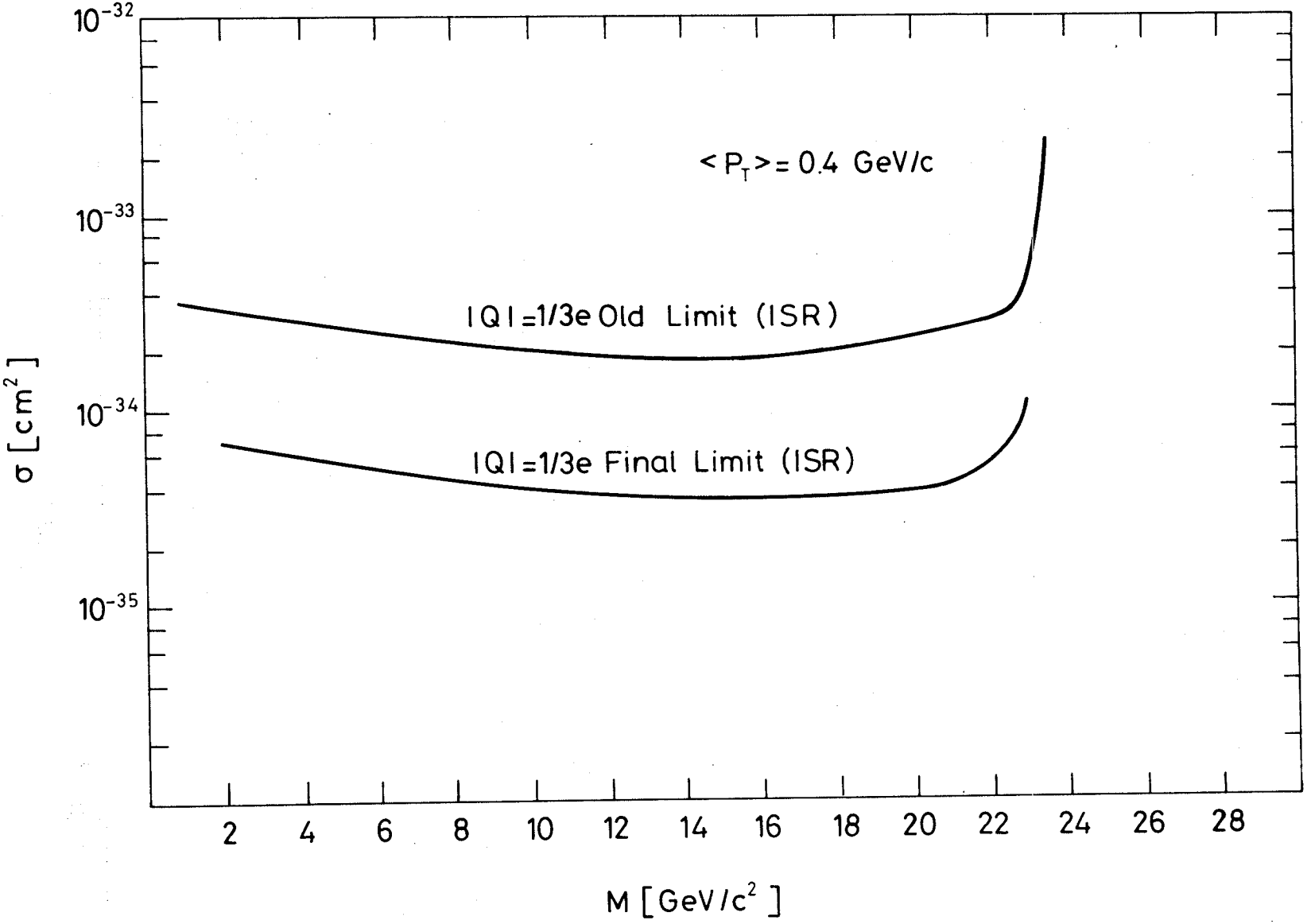
10^{-32}
10^{-33}
10^{-34}
10^{-35}
σ [cm^2]
$\langle P_T \rangle$ = 0.4 GeV/c
|Q|=1/3e Old Limit (ISR)
|Q|=1/3e Final Limit (ISR)
2 4 6 8 10 12 14 16 18 20 22 24 26 28
M [GeV/c^2]

Fig. 22

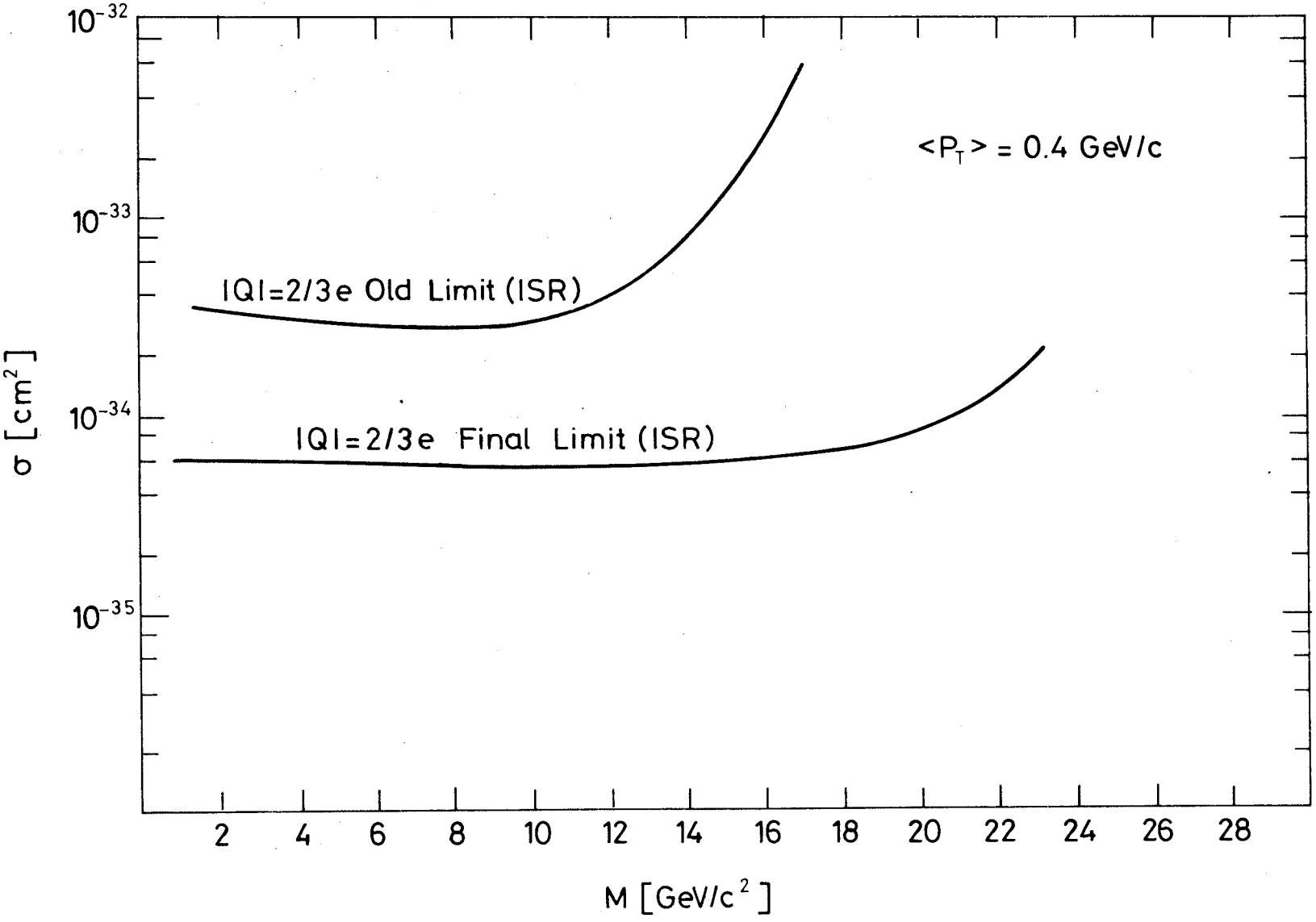
10^{-32}
10^{-33}
10^{-34}
10^{-35}
σ [cm^2]
$\langle P_T \rangle$ = 0.4 GeV/c
|Q|=2/3e Old Limit (ISR)
|Q|=2/3e Final Limit (ISR)
2 4 6 8 10 12 14 16 18 20 22 24 26 28
M [GeV/c^2]

Fig. 23